Eur. Phys. J. A **15**, 543–563 (2002)
DOI 10.1140/epja/i2002-10048-2

**THE EUROPEAN PHYSICAL JOURNAL A**

# Few-nucleon systems with two-nucleon forces from chiral effective field theory

E. Epelbaum[1,a], A. Nogga[2,b], W. Glöckle[1,c], H. Kamada[3,d], U.-G. Meißner[4,e], and H. Witała[5,f]

[1] Ruhr-Universität Bochum, Institut für Theoretische Physik II, D-44870 Bochum, Germany
[2] Department of Physics, University of Arizona, Tucson, AZ 85721, USA
[3] Department of Physics, Faculty of Engineering, Kyushu Institute of Technology, 1-1 Sensuicho, Tobata, Kitakyushu 804-8550, Japan
[4] Forschungszentrum Jülich, Institut für Kernphysik (Theorie), D-52425 Jülich, Germany
[5] Jagiellonian University, Institut of Physics, Reymonta 4, 30-059 Cracow, Poland

Received: 11 March 2002 /
Published online: 10 December 2002 – © Società Italiana di Fisica / Springer-Verlag 2002
Communicated by P. Schuck

**Abstract.** Nucleon-nucleon (NN) forces from chiral perturbation theory at next-to-leading (NLO) and next–to–next-to-leading order (NNLO) are applied to systems with two, three and four nucleons. At NNLO, we consider two versions of the chiral potential which differ in the strength of the two-pion exchange (TPE) but describe two nucleon observables equally well. The NNLO potential leads to unphysical deeply bound states in the low partial waves and effects of the 3N forces, which appear first at this order, are expected to be large. We provide arguments for a reduction of the TPE potential and introduce the NNLO* version of the NN forces. We calculate *nd* scattering observables as well as various properties of $^3$H and $^4$H with the NNLO* potential and find good agreement with the data and with predictions based upon the standard high-precision potentials. We find an improved description of the $^3$H and $^4$H binding energies.

**PACS.** 21.45.+v Few-body systems – 21.30.-x Nuclear forces – 27.10.+h $A \leq 5$ – 25.10.+s Nuclear reactions involving few-nucleon systems

## 1 Introduction

Nuclear forces are derived in the chiral effective field theory approach in terms of an expansion in powers of $Q/\Lambda_\chi$, where $Q$ corresponds to a generic external momentum of nucleons and $\Lambda_\chi$ represents the typical hadronic scale (scale of chiral symmetry breaking) of the order of 1 GeV. That ratio is less than one if one considers processes with sufficiently low external momenta of the nucleons. In order to exclude contributions of high-momentum components in intermediate states, the nucleon-nucleon (NN) potential is multiplied by a regulator, which suppresses momenta larger than a certain cut-off $\Lambda$ [1]. The latter has to be chosen below the scale $\Lambda_\chi$[1]. The cut-off $\Lambda$ should also not be taken too small in order not to suppress the relevant physics. The various coupling constants depend on the cut-off $\Lambda$ in a way to compensate the changes in the low-energy observables induced by varying $\Lambda$. The remaining cut-off dependence of the observables can be removed by adding higher-order terms to the effective potential [1]. Assuming naturalness for the various renormalized coupling constants in the underlying Lagrangian one can expect that contributions to the NN forces corresponding to higher powers $\nu$ of the chiral expansion will decrease. This sort of nuclear interactions based on the most general chiral invariant effective Lagrangian formed out of pion and nucleon fields has been first proposed in [4] and formulated in detail in [5]. We followed a similar path, however extracting the nuclear forces from the Lagrangian in a different way. We refer to [6] where two- and three-nucleon potentials have been derived using the method of unitary transformation. That method leads to energy

[a] e-mail: evgeni.epelbaum@tp2.ruhr-uni-bochum.de
[b] e-mail: anogga@physics.arizona.edu
[c] e-mail: walter.gloeckle@tp2.ruhr-uni-bochum.de
[d] e-mail: kamada@mns.kyutech.ac.jp
[e] e-mail: u.meissner@fz-juelich.de
[f] e-mail: witala@if.uj.edu.pl

[1] In some cases it turns out to be possible to perform standard renormalization of the theory by taking the cut-off $\Lambda$ to infinity [2,3].

independent and Hermitian nuclear forces which are better suited for applications to systems with $A > 2$ than energy-dependent forces derived in old-fashioned time-ordered perturbation theory like in [5]. In [7] we applied the forces at next-to-leading order (NLO), corresponding to (the counting index) $\nu = 2$, to the 3N and 4N systems. At this order NN phase shifts can be described only at rather low energies and only modestly. Nevertheless, 3N and 4N binding energies were found to be within the same range as the ones found with high-precision modern NN forces and also *nd* elastic and break-up observables at very low energies are similar to predictions generated by conventional forces. At that order the experimental nucleon analyzing power $A_y$ is fairly well reproduced, which for conventional NN forces poses a serious puzzle [8]. This result, however, has to be considered as an intermediate step, corresponding just to NLO, where the $^3P_j$ NN phase shifts could not be reproduced with sufficient accuracy. It is now of strong interest to explore the chiral forces in 3N and 4N systems at next–to–next-to-leading order (NNLO) corresponding to $\nu = 3$ where the NN phase shifts are better reproduced. For the convenience of the reader we review briefly the NN forces in LO ($\nu = 0$), NLO and NNLO in sect. 2.

It has been already pointed out in [9] that the strong central attraction caused by the numerically large values of the LECs $c_1$, $c_3$, and $c_4$ as determined in a $Q^3$ analysis of $\pi$N scattering leads to spurious deeply bound states in various two-nucleon angular-momentum states. Though this has no observable consequences in the NN system within the realm of validity of the theory it is technically somewhat disturbing in treating 3N and 4N systems. Also ignoring 3N forces, which occur at NNLO the first time, and exploring only the NNLO NN forces leads to strong deviations from 3N data as we will show. It has to be expected that this will be remedied by including the NNLO 3N forces, which necessarily have to be taken into account at that order. Various consequences of the large values of the $c_i$'s as well as the current situation in relation to the determination of the $c_i$'s from other processes (such as $\pi$N scattering) are discussed in sect. 3. Motivated by the findings of the boson exchange (BE) models of the nucleon-nucleon interaction, we constructed the NNLO* potential by removing the $\Delta$ content from the LECs $c_3$ and $c_4$ and refitting the contact interactions. The new values of the $c_i$'s resulting from subtracting the $\Delta$ contributions lead to the NNLO* potential which is free of spurious NN bound states for the cut-off range considered. The resulting NN phase shifts as shown in sect. 3 are significantly improved as compared to the NLO result. We also discuss in this section various deuteron properties. It should be mentioned that all these conclusions are based on the type of regulator we employ in the Lippmann-Schwinger equation. It cannot be excluded at present that a regulator can be constructed that allows for using the large $c_i$ without leading to deep virtual bound states. However, if such regularization exists, it has to look very different than the commonly employed regulator functions.

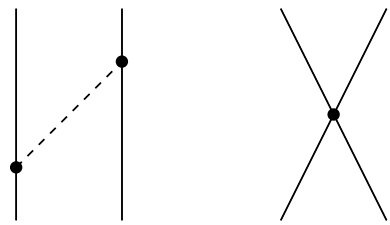

**Fig. 1.** Leading-order (LO) contributions to the NN potential: one-pion exchange and contact diagrams. Graphs which result from the interchange of the two-nucleon lines are not shown. Solid and dashed lines are nucleons and pions, respectively. The heavy dots denote the vertices with $\Delta_i = 0$.

We then switch to the 3N and 4N systems and briefly demonstrate in sect. 4 the predictions corresponding to the NNLO potential. As already stated before, neglecting the 3N forces leads to strong deviations from the data.

The central results of our paper, namely the application of the NNLO* potential to predict 3N and 4N observables, are presented in sect. 5. All these results have to be supplemented in the future by the inclusion of the three types of topologically different 3N forces which occur at NNLO. This additional extensive investigation is left to a forthcoming paper. We summarize briefly in sect. 6.

## 2 Few-nucleon forces in chiral effective field theory

Starting from the most general chiral invariant effective Hamiltonian density for pions and nucleons one can derive nuclear forces by eliminating the pions through a method of unitary transformation [6]. Since this transformation acts on the field-theoretical Hamiltonian, it leads to an energy-independent effective Hamiltonian in the pure nucleonic space. The condition for decoupling the purely nucleonic Fock space states from the ones with pions, a non-linear decoupling equation, can be linearized by introducing a series of orthonormal subspaces with different number of pions leading to an infinite set of coupled equations determining the unitary operator. Those equations can be solved recursively. Thereby the basic organization principle is a counting scheme in powers of momenta and number of pions. We refer to [6] for the detailed steps. Notice also that the relativistic $1/m$ corrections are assumed to be suppressed compared to the $1/\Lambda_\chi$ ones, see [4]. Further, we will consider only the isospin invariant case in this section. Isospin-violating effects can be treated along the lines presented in refs. [10,11]. The resulting nucleonic potentials are ordered by the power

$$\nu = -4 + E_n + 2L + \sum_i V_i \Delta_i, \tag{2.1}$$

where $E_n$, $L$ and $V_i$ are the numbers of external nucleon lines, loops and vertices of type $i$, respectively. Further, the quantity $\Delta_i$, which defines the dimension of a vertex of type $i$, is given by

$$\Delta_i = d_i + \frac{1}{2} n_i - 2, \tag{2.2}$$

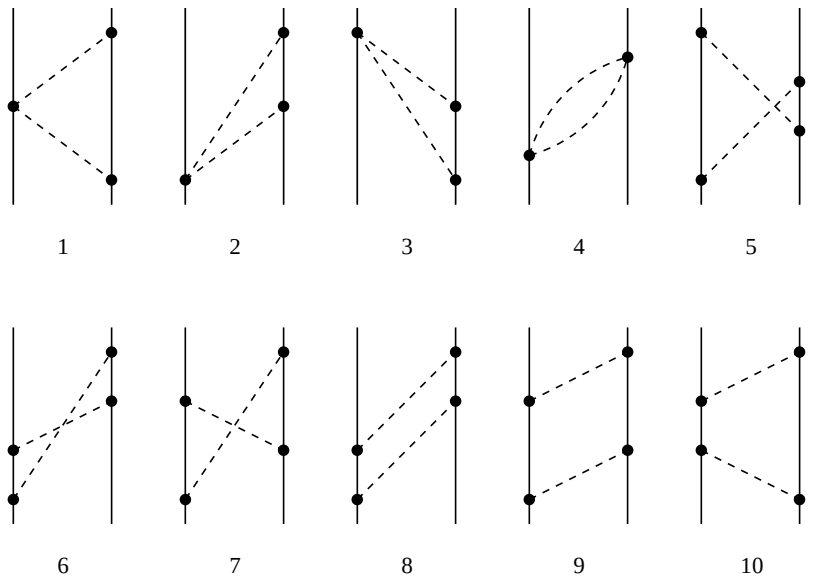


**Fig. 2.** First corrections at NLO to the NN potential in the projection formalism: two-pion exchange diagrams. For notations see fig. 1.

with $d_i$ the number of derivatives or $M_\pi$ insertions and $n_i$ the number of nucleon lines at the vertex $i$. The inequality $\Delta_i \geq 0$ holds true as a consequence of chiral invariance. This leads to $\nu \geq 0$ for processes with two and more nucleons. One also recognizes that the diagrams with loops are suppressed and that $(n+1)$-nucleon forces appear at higher orders than $n$-nucleon forces.

Let us now consider first several orders of the NN force. At leading order $\nu = 0$ (LO) only tree diagrams with vertices of $\Delta_i = 0$ ($\pi$NN vertex with one derivative and two independent four-nucleon contact interactions without derivatives) are allowed, see eq. (2.1). Consequently, the LO chiral potential is given by the well-established one-pion exchange (OPE) and contact forces with the low-energy constants (LECs) $C_S$ and $C_T$, as shown in fig. 1

$$V^{(0)}_{\rm cont} = C_S + C_T \sigma_1 \cdot \sigma_2,$$
$$V^{(0)}_{\rm OPEP} = -\left(\frac{g_A}{2f_\pi}\right)^2 \boldsymbol{\tau}_1 \cdot \boldsymbol{\tau}_2 \frac{\vec{\sigma}_1 \cdot \vec{q}\,\vec{\sigma}_2 \cdot \vec{q}}{q^2 + M_\pi^2}. \qquad (2.3)$$

Here $\vec{p}$ and $\vec{p}\,'$ are the initial and final momenta of the nucleons in the CM frame and $\vec{q} = \vec{p}\,' - \vec{p}$. Further, $M_\pi$, $g_A$, and $f_\pi$ are the pion mass, the axial pion-nucleon coupling constant and the pion decay constant, respectively.

At next-to-leading order (NLO) or $\nu = 2$ there are TPE diagrams with the leading $\pi$NN vertices with $\Delta_i = 0$ according to fig. 2 and seven contact forces with vertices of $\Delta_i = 2$ containing two derivatives[2], see fig. 3. It should be emphasized at this stage, that the expression (2.1) only allows to estimate the order of the corresponding process. It is, however, not possible to read off the precise structure of the operators (*i.e.* the corresponding energy denominators and overall factors) related to a particular diagram. This is because the presented figures refer to diagrams within the method of unitary transformation and not to ordinary graphs in the old-fashioned perturbation theory. The precise operator form of the NLO and NNLO contributions to the 2N and 3N potentials can be found in ref. [6]. Note also that the graphs 9 and 10 in fig. 2 are not reducible ones in the sense that no energy denominators related to purely nucleonic intermediate states appear in the corresponding expressions; see [6] for more details.

In addition, there are nucleon self-energy contributions and vertex corrections [6], which renormalize the one-pion exchange and contact forces, which we do not show explicitly here. The TPE terms shown in fig. 2 lead to polynomial parts with, in general, infinite coefficients, which renormalize various contact interactions, and to finite non-polynomial ones, which are finite and independent of the

**Fig. 3.** First corrections to the NN potential: contact diagram at next-to-leading order (NLO). The filled diamond denotes seven vertices of $\Delta_i = 2$ (with two derivatives). For remaining notations see fig. 1.

[2] The contact interactions with one insertion of $M_\pi^2$ are formally indistinguishable from the four-nucleon operators without derivatives and lead to renormalization of the constants $C_S$, $C_T$. We will not consider such operators explicitly.

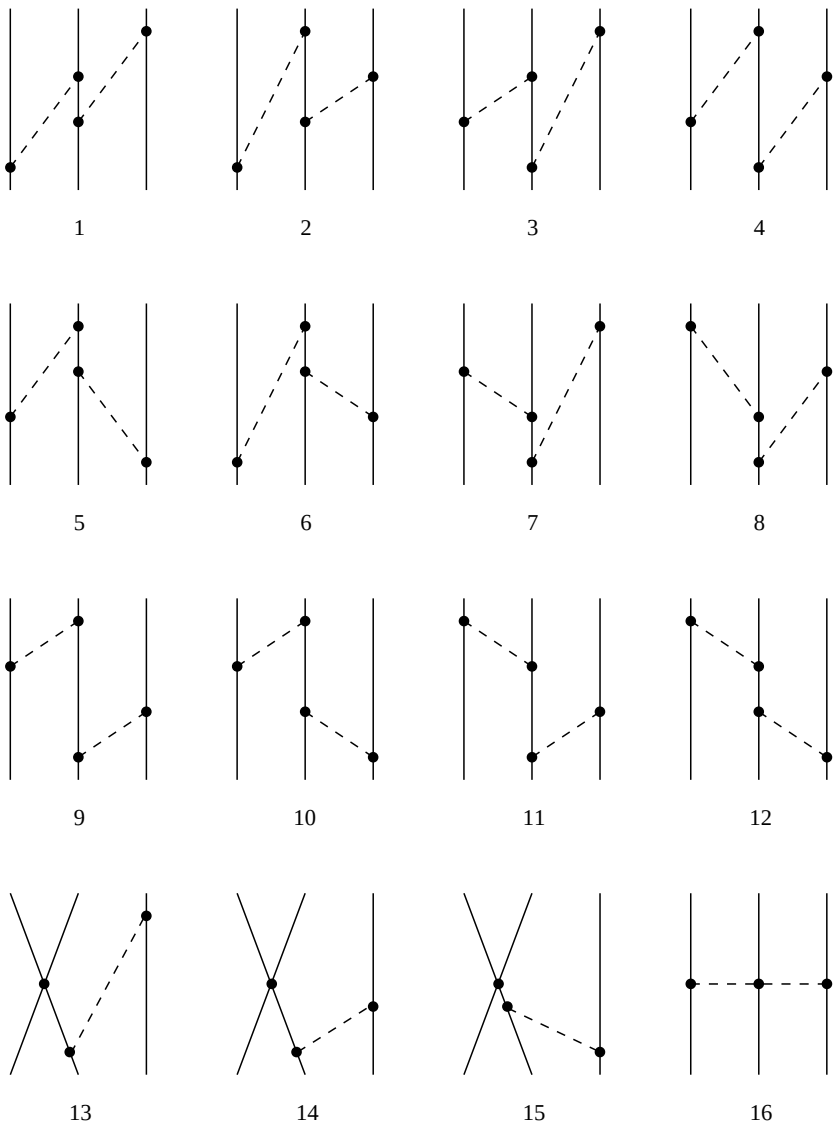


**Fig. 4.** Leading contributions to the three-nucleon potential at NLO, which cancel: two-pion and one-pion exchange diagrams with the NN contact interaction. Graphs which result from the interchange of the nucleon lines and/or from the application of time reversal operation are not shown. In the case of diagram 16, one should sum over all possible time orderings. For remaining notations see fig. 1.

regularization scheme used. The resulting potential reads

$$\begin{aligned} V^{(2)}_{\rm cont} &= C_1\vec{q}^{\,2} + C_2\vec{k}^{\,2} + \big(C_3\vec{q}^{\,2} + C_4\vec{k}^{\,2}\big)(\vec{\sigma}_1\cdot\vec{\sigma}_2) \\ &\quad + iC_5\frac{1}{2}(\vec{\sigma}_1+\vec{\sigma}_2)\cdot(\vec{q}\times\vec{k}) \\ &\quad + C_6(\vec{q}\cdot\vec{\sigma}_1)(\vec{q}\cdot\vec{\sigma}_2) + C_7(\vec{k}\cdot\vec{\sigma}_1)(\vec{k}\cdot\vec{\sigma}_2), \\ V^{(2)}_{\rm TPEP} &= -\frac{\boldsymbol{\tau}_1\cdot\boldsymbol{\tau}_2}{384\pi^2 f_\pi^4}L(q)\Big\{4M_\pi^2(5g_A^4-4g_A^2-1) \\ &\quad + q^2(23g_A^4-10g_A^2-1) + \frac{48g_A^4M_\pi^4}{4M_\pi^2+q^2}\Big\} \\ &\quad - \frac{3g_A^4}{64\pi^2 f_\pi^4}L(q)\big\{\vec{\sigma}_1\cdot\vec{q}\,\vec{\sigma}_2\cdot\vec{q} - q^2\vec{\sigma}_1\cdot\vec{\sigma}_2\big\}, \end{aligned} \tag{2.4}$$

where

$$L(q) = \frac{1}{q}\sqrt{4M_\pi^2+q^2}\,\ln\frac{\sqrt{4M_\pi^2+q^2}+q}{2M_\pi}\,, \tag{2.5}$$

and $\vec{k} = 1/2(\vec{p}\,' + \vec{p})$. There are seven LECs $C_1$ to $C_7$ related to contact interactions with two derivatives, see fig. 3.

At that order NLO 3N forces of the topologies shown in fig. 4 cancel. Note that this cancellation is of different type than the one found in time-ordered perturbation theory [12,13]. To be more precise, in that order the contribution of the "irreducible" two-pion (one-pion) exchange diagrams 1–8 (13) cancels against the "reducible" two-pion (one-pion) exchange graphs 9–12 (14, 15). The last graph 16 in this figure is proportional to the kinetic

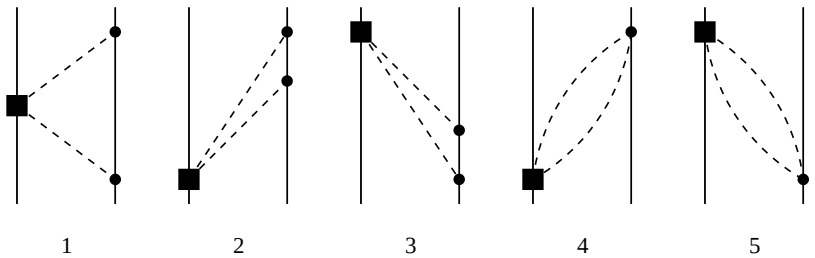


**Fig. 5.** Next–to–next-to-leading order (NNLO) corrections to the NN potential. The filled squares denote the vertices with $\Delta = 1$. For remaining notations see figs. 1, 3.

energy of the nucleons and contributes therefore only at higher orders [4].

At NNLO ($\nu = 3$) there occur new $\pi\pi$NN vertices with $\Delta_i = 1$, which contain either two derivatives or one $M_\pi^2$ insertion and are parametrized by three constants, denoted in the commonly used notation by $c_1$, $c_3$, and $c_4$ (the $c_2$-term does not contribute at this order) [14]. They enter into the TPE NN force as shown in fig. 5 as well as into vertex correction diagrams (not shown), which renormalize the OPE, and also into the TPE 3N force shown in fig. 6. The explicit expression for the two-pion exchange NN force at NNLO is[3]

$$
\begin{aligned}
V^{(3)}_{\rm TPEP} = &-\frac{3g_A^2}{16\pi f_\pi^4}\Bigg\{-\frac{g_A^2 M_\pi^5}{16m(4M_\pi^2+q^2)} \\
&+\left(2M_\pi^2(2c_1-c_3)-q^2\left(c_3+\frac{3g_A^2}{16m}\right)\right)\left(2M_\pi^2+q^2\right)A(q)\Bigg\} \\
&-\frac{g_A^2}{128\pi m f_\pi^4}(\boldsymbol{\tau}_1\cdot\boldsymbol{\tau}_2)\Bigg\{-\frac{3g_A^2 M_\pi^5}{4M_\pi^2+q^2} \\
&+\left(4M_\pi^2+2q^2-g_A^2\left(4M_\pi^2+3q^2\right)\right)\left(2M_\pi^2+q^2\right)A(q)\Bigg\} \\
&+\frac{9g_A^4}{512\pi m f_\pi^4}\left((\vec\sigma_1\cdot\vec q)(\vec\sigma_2\cdot\vec q)-q^2(\vec\sigma_1\cdot\vec\sigma_2)\right) \\
&\times(2M_\pi^2+q^2)A(q) \\
&-\frac{g_A^2}{32\pi f_\pi^4}(\boldsymbol{\tau}_1\cdot\boldsymbol{\tau}_2)\left((\vec\sigma_1\cdot\vec q)(\vec\sigma_2\cdot\vec q)-q^2(\vec\sigma_1\cdot\vec\sigma_2)\right) \\
&\times\left\{\left(c_4+\frac{1}{4m}\right)\left(4M_\pi^2+q^2\right)-\frac{g_A^2}{8m}\left(10M_\pi^2+3q^2\right)\right\}A(q) \\
&-\frac{3g_A^4}{64\pi m f_\pi^4}i(\vec\sigma_1+\vec\sigma_2)\cdot(\vec p\,'\times\vec p)\left(2M_\pi^2+q^2\right)A(q) \\
&-\frac{g_A^2(1-g_A^2)}{64\pi m f_\pi^4}(\boldsymbol{\tau}_1\cdot\boldsymbol{\tau}_2)i(\vec\sigma_1+\vec\sigma_2)\cdot(\vec p\,'\times\vec p) \\
&\times\left(4M_\pi^2+q^2\right)A(q), \qquad (2.6)
\end{aligned}
$$

where

$$A(q) = \frac{1}{2q}\arctan\frac{q}{2M_\pi}\,. \qquad (2.7)$$

Altogether there are 9 LECs at NNLO (and at NLO) related to various contact interactions, which have to be fitted by adjusting the NN force to the NN data. The LECs $c_{1,3,4}$ which first appear at NNLO occur also in $\pi$N scattering and that information should be consistently taken into account.

[3] Note that we included here the $1/m$ corrections, which are formally of higher order.

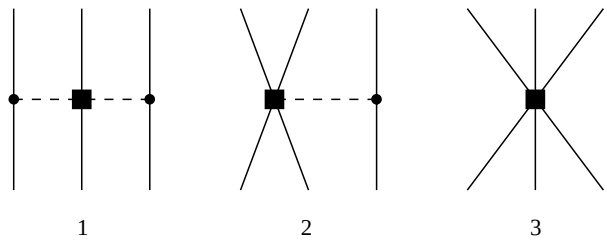


**Fig. 6.** Three-nucleon force: TPE, OPE and contact interaction. In the cases of diagrams 1 and 2, all possible time orderings should be taken into account. For notations see figs. 1 and 5.

The 3N force at NNLO consists of three different topologies as shown in fig. 6. Besides the TPE there is a pion exchange between a NN contact force and the third nucleon and a pure 3N contact force. In both cases new vertices of $\Delta_i = 1$ with unknown constants enter. The precise structure of the chiral 3NF will be discussed in a forthcoming paper.

Chiral forces are only valid in a low-momentum region. We enforce this by modifying the above given NN force expressions as

$$V(\vec p\,',\vec p) \longrightarrow f_{\rm R}(\vec p\,')V(\vec p\,',\vec p)f_{\rm R}(\vec p), \qquad (2.8)$$

where $f_{\rm R}(\vec p)$ is a regulator function. In what follows, we work with the following regulator function:

$$f_{\rm R}^{\rm expon}(\vec p) = \exp\left[-p^4/\Lambda^4\right]. \qquad (2.9)$$

The power four in the exponent guarantees that the $Q^0$-, $Q^2$- and $Q^3$-terms in the potential are not affected by the regularization procedure. As already pointed out before, the dependence of the low-energy observables on the value of the cut-off $\Lambda$ should get weaker with increasing the order $\nu$.

## 3 Two nucleons at next–to–next-to-leading order

We now turn to the analysis of the 2N system at NNLO. Let us first specify the parameters entering the NN potential. The largest uncertainty is related to contact interactions between nucleons. They are not restricted by

chiral symmetry, but only by the general principles of locality, invariance under Lorentz transformations, parity, time-reversal invariance and Hermiticity. At NLO and NNLO one has to take into account nine independent contact operators contributing to the effective potential: two operators without derivatives ($V^{(0)}_{\rm cont}$ in eq. (2.3)) and seven with two derivatives of nucleon fields ($V^{(2)}_{\rm cont}$ in eq. (2.4)). The corresponding LECs are fixed by a fit to $S$- and $P$-wave phase shifts and to $\epsilon_1$ at low energies. The OPE ($V^{(0)}_{\rm OPEP}$ in eq. (2.3)) as well as the leading chiral TPE at NLO ($V^{(2)}_{\rm TPEP}$ in eq. (2.4)) are parameter free.

As already stressed before, the subleading TPE at NNLO, $V^{(3)}_{\rm TPEP}$ in eq. (2.6), depends on the LECs $c_{1,3,4}$, which correspond to $\pi\pi$NN vertices of dimension $\Delta_i = 1$. Precise numerical values for these constants are crucial for various properties of the effective NN interaction as will be discussed below. Clearly, the subleading $\pi\pi$NN vertices represent an important link between NN scattering and other processes, such as $\pi$N scattering. Therefore, ideally, one would like to take their values from the analysis of the $\pi$N system, as was done in [9]. We will now briefly overview the current situation concerning the determination of the $c_i$'s from the $\pi$N system. Several calculations for $\pi$N scattering have been performed and published. From the $Q^2$ analysis [15] one gets: $c_1 = -0.64$, $c_3 = -3.90$, $c_4 = 2.25$. Here all values are given in GeV$^{-1}$. From different $Q^3$ calculations [15–19] one obtains the following bands for the $c_i$'s:

$$c_1 = -0.81 \ldots -1.53, \quad c_3 = -4.70 \ldots -6.19, \quad c_4 = 3.25 \ldots 4.12. \tag{3.1}$$

These bands are also consistent with expectations from resonance saturation, see [16]. Recently, the results from a $Q^4$ analysis have become available [20]. At this order the $S$-matrix is sensitive to 14 LECs (including $c_{1,3,4}$), which have been fixed from a fit to $\pi$N phase shifts. At this order the dimension two LECs acquire a quark mass renormalization. The corresponding shifts are proportional to $M_\pi^2$. It turns out that different phase shift analyses (PSA) from refs. [21–23] lead to sizable variations in the actual values of the LECs. A typical fit based on the phases of ref. [22] leads to

$$\tilde{c}_1 = -0.27 \pm 0.01, \quad \tilde{c}_3 = -1.44 \pm 0.03, \quad \tilde{c}_4 = 3.53 \pm 0.08, \tag{3.2}$$

where $\tilde{c}_i$ denote the renormalized $c_i$'s. However, using the older Karlsruhe or the VPI phases as input, one finds sizable variations in the $\tilde{c}_i$. Alternatively, one can also keep the $c_i$ at their third-order values and fit the fourth-order corrections separately, see [20]. Due to the uncertainties in the isoscalar amplitudes, these constants are not very well determined. The fits could, in principle, be improved in the future by including the scattering lengths determined from pionic hydrogen/deuterium. To complete the discussion on determination of the $c_i$'s from the $\pi$N system we would like to stress that numbers consistent with the bands given in eq. (3.1) have been obtained in [24] using IR regularized baryon chiral perturbation theory at order $Q^3$ and dispersion relations.

Rentmeester *et al.* [25] tried to fix the values of the $c_i$'s from an analysis of the $pp$ data, which are of a much better quality than the $\pi$N data. In this approach the long-range part of the NN force was taken as the sum of the OPE and the chiral TPE (including the NNLO contribution). The NN interaction at short distances below some boundary value was parametrized by some artificial energy-dependent representation. The global fit to the data allowed to pin down the values of the $c_i$'s (and, of course, also of the parameters related to the short-range part of the NN force). It turned out that it is not possible to fix all three $c_i$'s in this process because of the strong correlation between these LECs. For that reason the constant $c_1$ was fixed at the value $c_1 = -0.76\,\text{GeV}^{-1}$ (to obtain a small pion-nucleon $\sigma$-term of about 40 MeV) and the LECs $c_{3,4}$ were treated as free parameters. The values of the $c_{3,4}$: $c_3 = -5.08\,\text{GeV}^{-1}$, $c_4 = 4.70\,\text{GeV}^{-1}$ determined from the global fit to the $pp$ data are compatible with the $Q^3$ calculation from the $\pi$N system, see eq. (3.1). Note, however, that this method is not directly based on a systematic chiral power counting.

Having overviewed the current status of the determination of the $c_i$'s from various processes, we are now in the position to discuss the corresponding implications for the NN system. First of all, it turns out that the numerical values of the $c_i$'s are quite large. Indeed, from a dimensional analysis one would expect, for example, the constant $c_3$ to scale like

$$c_3 \sim \frac{\ell}{2\Lambda_\chi}\,, \tag{3.3}$$

where $\ell$ is some number of order one. Taking the value $c_3 = -4.70$ from ref. [19] and $\Lambda_\chi = M_\rho = 770\,\text{MeV}$ we end up with $\ell \sim -7.5$. Such a large value can be partially explained by the fact that the $c_{3,4}$ are to a large extent saturated by the $\Delta$ excitation. This implies that a new and smaller scale, namely $m_\Delta - m \sim 293\,\text{MeV}$, enters the values of these constants, see [16].

What are the consequences of the large numerical values of the $c_i$'s for NN scattering? The main problem is that the large numerical values of the $c_i$'s might lead to a slow convergence of the low-momentum expansion. To get a feeling of the possible problems one can compare, for instance, the low-momentum matrix elements of, say, the central parts of the TPE at NLO and NNLO. Taking the values of the $c_i$'s from the $Q^3$ analysis of the $\pi$N system from ref. [19]

$$c_1 = -0.81\,\text{GeV}^{-1}, \quad c_3 = -4.70\,\text{GeV}^{-1}, \quad c_4 = 3.40\,\text{GeV}^{-1}, \tag{3.4}$$

as we did in [9] one gets from eqs. (2.4), (2.6):

$$V^{\text{cent, }(2)}_{\rm TPE}(q)\Big|_{q=0} = (\boldsymbol{\tau}_1\cdot\boldsymbol{\tau}_2)\frac{M_\pi^2}{(4\pi f_\pi)^2 f_\pi^2}\frac{\left(1+4g_A^2-8g_A^4\right)}{6} \sim (\boldsymbol{\tau}_1\cdot\boldsymbol{\tau}_2)(-3.4)\,\text{GeV}^{-2}, \tag{3.5}$$

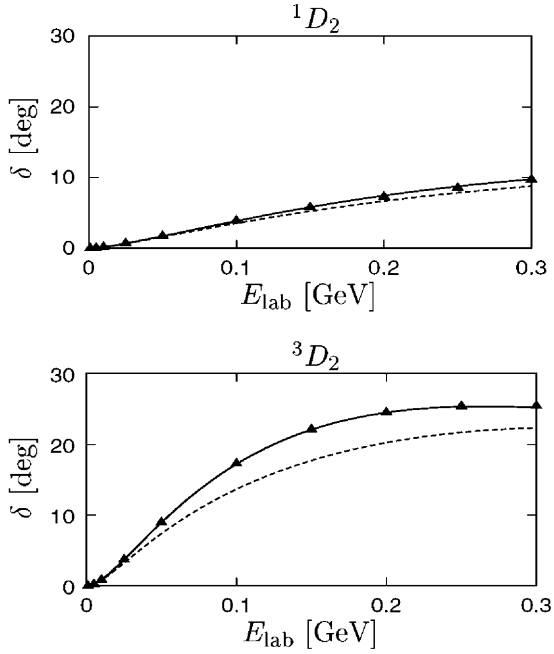


**Fig. 7.** $^1D_2$ and $^3D_2$ phase shifts calculated with the CD-Bonn potential. The dashed lines show the Born approximation, whereas the solid lines correspond to the full solution of the Lippmann-Schwinger equation. The filled triangles are Nijmegen PSA results [26].

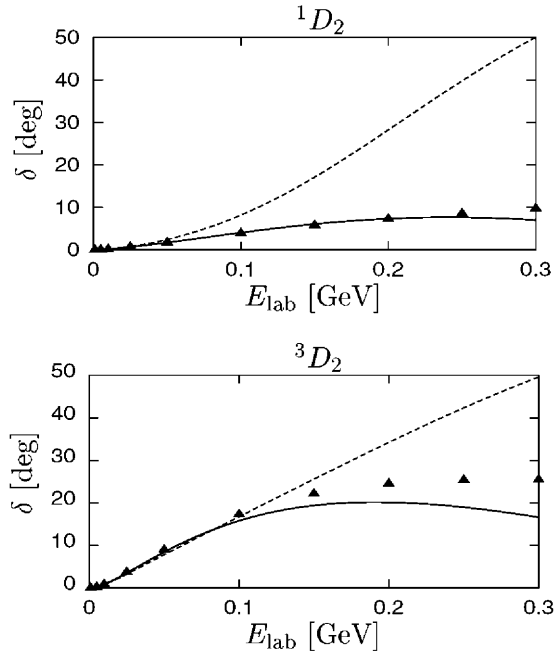


**Fig. 8.** $^1D_2$ and $^3D_2$ phase shifts at NNLO using the values of the $c_i$'s from ref. [19]. The dashed lines show the Born approximation, whereas the solid lines correspond to the iterated solution with the exponential cut-off $\Lambda = 1000\,\mathrm{MeV}$. The filled triangles are Nijmegen PSA results [26].

$$V_{\rm TPE}^{\rm cent,\,(3)}(q)\Big|_{q=0} = \frac{M_\pi^2}{(4\pi f_\pi)^2 f_\pi^2}\big(-3g_A^2\pi\big)(2c_1-c_3)M_\pi \sim -10.3\,\mathrm{GeV}^{-2}. \tag{3.6}$$

Here we neglected all $1/m$ corrections. While the order of the matrix element of the potential at NLO agrees with the one expected from dimensional analysis, $V_{\rm TPE}^{\rm cent,\,(2)} \sim (\boldsymbol{\tau}_1\cdot\boldsymbol{\tau}_2)\ell_1 M_\pi^2/(\Lambda_\chi^2 f_\pi^2)$ with $\ell_1 \sim -0.9$, the NNLO matrix element appears to be larger than expected: $V_{\rm TPE}^{\rm cent,\,(3)} \sim \ell_2 M_\pi^3/(\Lambda_\chi^3 f_\pi^2)$, where $\ell_2 \sim -14.3$. Such a deviation from the natural value for $\ell_2$ of order one does, however, not yet necessarily mean a failure of the perturbative expansion, since the potential itself is not an observable quantity. To draw a precise conclusion about the convergence properties of the low-momentum expansion one should look at the phase shifts, which can be measured directly. Further, up to now we only compared the non-polynomial contributions to the potential and omitted all contact terms[4]. Large numerical values of the low-momentum matrix elements of the $V_{\rm TPE}$ at NNLO could, in principle, be compensated by the corresponding contact terms. However, such a compensation at NNLO is only possible for $S$- and $P$-waves as well as for $\epsilon_1$ since the contact terms do not contribute to $D$ and higher partial waves at this order. The $D$- and $F$-waves may therefore serve as a sensitive test of the chiral TPE exchange[5]. The conventional scenario of nuclear forces represented by existing OBE models and various phenomenological potentials suggests that the $D$- and higher partial-wave NN interactions are weak enough to be treated perturbatively. This is demonstrated in fig. 7 on the example of the CD-Bonn potential. Although this observation is confirmed by the smallness of the corresponding phase shifts, such a scenario, strictly speaking, does not necessarily need to be realized. In fact, the NNLO results can serve as a counter example: with the values of the $c_i$'s from eq. (3.4), the Born approximation for the $S$-matrix, for instance, in the $^1D_2$ partial wave deviates strongly from the data already at $E_{\rm lab} \sim 100\,\mathrm{MeV}$, see fig. 8. Note that this result is parameter free and cut-off independent[6]. Similar results have been published in ref. [27]. On the other hand, as we showed in [9], taking the cut-off of the order of 1 GeV allows for a satisfactory description of all partial waves simultaneously. With such a large value of the cut-off, the central TPE potential becomes already so strongly attractive that unphysical deeply bound states appear in the $D$-waves as well as in the lower partial waves. Since the potential is very strong (and attractive) and there are no counter terms

[4] Note that the contact interactions are needed to renormalize the TPE contribution and thus cannot be omitted for conceptual reasons.

[5] This has been suggested by Kaiser *et al.* in [27,28].

[6] Since we do not iterate the potential, we do not need to multiply it with the regulating function. Strictly speaking, of course, the EFT is only defined with the cut-off procedure which would lead to the results in Born approximation being multiplied with an overall factor. For simplicity, we ignore this factor here.

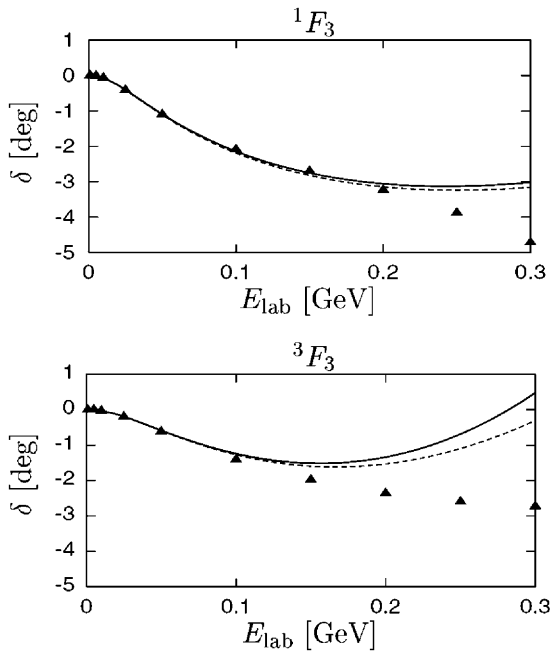


**Fig. 9.** $^1F_3$ and $^3F_3$ partial waves at NNLO using the values of the $c_i$'s from ref. [19]. For notations, see fig. 8. The filled triangles are Nijmegen PSA results [26].

according to the power counting, changing the value of the cut-off clearly leads to strong variation of the $D$-wave phase shifts. This is illustrated and discussed in more detail in [9,29]. Note that this problem of the strong cut-off dependence does not show up in lower partial waves, where it is compensated by the cut-off dependence of the contact counter terms. In the $F$-waves, where the potential is already sufficiently weak (if the cut-off $\Lambda$ is chosen smaller or of the order of 1 GeV) and the Born approximation already does a good job, one has no problems with the cut-off dependence as well. This is shown in fig. 9. In spite of this fact one observes sizable deviations for most of the $F$-wave phase shifts from the Nijmegen PSA for energies larger than $E_{\rm lab} \sim 150\,$MeV [9]. Thus, the only serious difficulty caused by the large values of the $c_i$'s in the NNLO analysis of the NN system is related to the cut-off dependence of the $D$-wave phase shifts.

The large numerical values of the $c_i$'s have also some consequences for three- and more-nucleon systems, which will be discussed in detail in the next section. Here we only emphasize that effects from the inclusion of the 3N forces are expected to be much larger than in the standard scenario of nuclear physics. Note, however, that the separate contributions of the 2N and 3N forces to 3N observables cannot be measured experimentally.

Let us now briefly summarize the consequences of the inclusion of the NNLO TPE with the large values of the $c_i$'s taken from the $Q^3$ analysis of the $\pi$N system [19]:

- First of all, including the subleading TPE allows for significant improvement in the description of the low-energy observables in the NN system compared to NLO without introducing additional parameters, see ref. [9] for more details. The phase shifts are mostly well reproduced.
- The central part of the potential shows a much stronger attraction than the one found in conventional models of the NN interaction [27]. As a consequence, one has unphysical deeply bound states in the low NN partial waves.
- The predictions for $D$-waves depend on the cut-off. The optimal result is obtained for $\Lambda = 1000\,$MeV using the exponential regulator. The potential projected onto the $D$-waves is strong and requires non-perturbative summation via the Lippmann-Schwinger equation. The predictions for $F$-waves deviate from the data at energies larger than $E_{\rm lab} \sim 150\,$MeV. In contrast, the peripheral waves are well described [27].
- One expects large effects from the 3NF.

Although the NNLO scenario dictated by the large values of the $c_i$'s differs strongly from our expectations based on the experience with various phenomenological boson exchange models, one cannot exclude this possibility *a priori*. Indeed, the only serious problem with the large $c_i$'s is given by the strong cut-off dependence of the $D$-wave phase shifts. However, this will probably not (or only weakly) affect chiral predictions for experimentally measured quantities like the cross-section, analyzing powers, etc. at low energies, where the contribution of the corresponding phases to physical observables is rather small. Further, as already discussed in detail in ref. [9], at N$^3$LO it will be cured by dimension four contact interactions. Furthermore, the failure of the NNLO potential to describe various properties in the 3N and 4N systems does not yet indicate a problem, since we have not included the 3NF. Because of the calculational difficulties in the treatment of the 3N and 4N systems in the presence of deeply bound states it will take some time before all the implications of the chiral EFT at NNLO using the large values of the $c_i$ are explored in detail. These calculations need to be done but will require a large amount of computing time.

Having discussed consequences of the large values of the $c_i$'s for various properties of few-nucleon systems, we can ask ourselves, how confident we are, that the discussed scenario is indeed realized? Several comments are in order:

- First of all, we would like to stress the uncertainty in the determination of the $c_i$'s from $\pi$N scattering. The difference between the $c_i$'s from the second- and third-order analyses of $\pi$N scattering is considered to be an effect of third order, *i.e.* it should be suppressed by one power of $Q$ compared to the second-order values of the $c_i$'s. For that reason one can equally well take the $Q^2$-values of the $c_i$'s in the NNLO analysis of the NN system, since the $c_i$'s enter only the NNLO and not the NLO contribution to the effective potential. In principle, one can also take the values of the $\tilde{c}_i$ from the $Q^4$ analysis, which differ from the $c_i$'s by quark mass renormalizations of the order $M_\pi^2$. Taking different sets of the $c_i$'s from various analyses of the $\pi$N system, as described in the beginning of this section, might not cause significant variation in description of low-energy

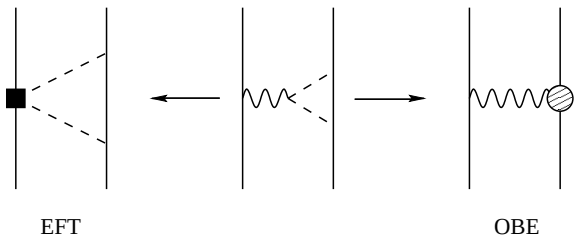


**Fig. 10.** Exchange of $\rho$-meson (wiggly line), which decays into two pions (dashed lines) and the corresponding diagrams in EFT (left-hand panel) and OBE models (right-hand panel). The shaded blob represents the strong $\rho$N form factor in OBE models. For remaining notations see figs. 1, 5.

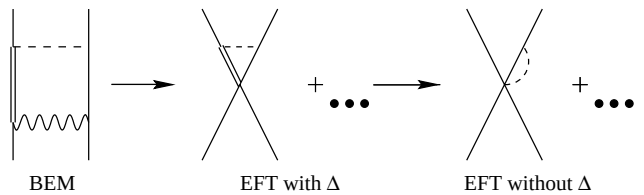


**Fig. 11.** Representation of the $\pi\rho$ exchange diagram within EFT approaches with and without explicit $\Delta$. BEM stays for boson exchange models. For notations see fig. 10.

observables in the $\pi$N as well as NN systems, but lead to different scenarios.

– It is also possible that including higher-order loop effects will reduce the strength of the central part of effective NN potential even if the $c_i$'s are numerically large.
– Finally, already at N$^3$LO one has to include new contact interactions with four derivatives, which also contribute in $D$-waves. These will not only reduce the cut-off dependence of the phase shifts, but may also provide additional repulsion and allow to avoid unphysical deeply bound states. The work by Entem and Machleidt [30], who constructed a NN potential without deeply bound states by a phenomenological extension of the NNLO chiral NN force[7], may serve as an indication of the importance of the higher-order contact interactions. To ultimately clarify the situation one has to perform a complete analysis of the NN system at order N$^3$LO.

It is interesting to understand the reason of (possibly) different scenarios in the EFT approach and in more phenomenological conventional boson exchange (BE) models. It has been pointed out in ref. [16] that the LECs $c_{3,4}$ get the dominant contributions from the intermediate $\Delta$ excitation. Also, the $\sigma$- and $\rho$-mesons have been shown to play an important role in the saturation of the $c_i$'s. In particular, the constant $c_1$ is completely saturated by the $\sigma$ [16]. Let us now check whether these mechanisms of resonance saturation of the $c_i$'s are also realized in the OBE models of the NN interaction. While the resonance saturation of the $c_i$'s by heavy mesons can, in principle, be interpreted in terms of OBE contributions as shown in fig. 10, where the pion loop in the graph in the middle of that figure contributes to the form factor of the corresponding heavy meson, the saturation by the $\Delta$ excitation cannot be represented in an appropriate way within the OBE models. Thus, a large portion of the subleading chiral TPE is absent in the conventional NN forces.

A more detailed investigation of the two-pion exchange within the conventional many-boson exchange formalism gives rise to a better understanding of the reasons why the intermediate $\Delta$ plays only a modest role in the NN interaction. In the Bonn model of ref. [31], which also allows for two-boson exchanges, one finds strongly attractive contributions from TPE. Note that this model also takes into account $\Delta$ excitations in the intermediate states. The diagrams with intermediate $\Delta$ excitations have been shown to give the dominant contribution to the uncorrelated TPE. While the TPE model successfully describes high angular-momentum partial waves, quantitative description of low partial waves appears to be impossible. It is even stated in ref. [31] that "the $2\pi$-contribution appears, in general, too attractive and a consistent and quantitative description of all phase shifts can never be reached". It was shown that the strongly attractive contribution of the TPE in low partial waves is to a large extent cancelled by the $\pi\rho$ diagrams. The authors of ref. [32] came to a similar conclusion. The more detailed work on correlated $\pi\rho$ exchange has been performed within the conventional formalism by Holinde and collaborators, see [33]. In fig. 11 we show one specific example of the $\pi\rho$ exchange with the corresponding representation in the EFT approach. It is easy to see that the NLO[8] contribution to the effective potential from the diagram shown in fig. 11 only leads to renormalization of the corresponding LO contact interactions and thus will only influence the $S$-wave phase shifts. Thus, one needs to go to higher orders beyond NNLO in the low-momentum expansion to see effects of the $\pi\rho$ exchange on the phase shifts in $P$- and $D$-waves. The better way to observe the cancellation between the $\pi\pi$ and $\pi\rho$ exchanges might be to include vector mesons as explicit degrees of freedom in the EFT. That would however require a consistent power-counting scheme, which has not yet been constructed.

The study of the TPE within the Bonn model [35] also indicates a very important role of relativistic effects for diagrams with intermediate $\Delta$'s. Incorporating relativistic corrections using IR regulated covariant baryon CHPT [36] within the EFT formalism has already been shown to reduce the strength of the subleading TPE by about 30% [37].

Although phenomenological boson exchange models provide a plausible explanation of the fact that the $\Delta$-resonance does not play a significant role in NN scattering, additional model-independent analysis is needed to improve on our understanding of the TPE. In particular,

[7] To be precise, they included the N$^3$LO contact interactions and allowed for a partial-wave dependent cut-off variation. Thus, this extension is *not* an EFT approach.

[8] Note that if the $\Delta$-resonance is included explicitly via the "small scale expansion" [34], the strong attractive central contribution to the TPE appears already at NLO and not at NNLO.

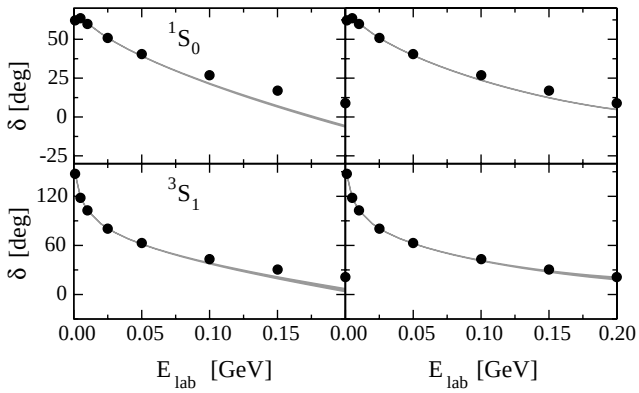


**Fig. 12.** Fits and predictions for the $S$-waves for nucleon laboratory energies $E_{\rm lab}$ below 200 MeV (0.2 GeV). Left/right panels: NLO/NNLO* results. The cut-off is chosen between 500 and 600 MeV leading to the band. The filled circles depict the Nijmegen PSA results [26].

more work on pion-nucleon scattering (dispersive *versus* chiral representation), new dispersive analyses and more precise low-energy data are needed to pin down these LECs to the precision required here.

Motivated by the observed cancellation between the $\pi\pi$ and $\pi\rho$ exchanges and by the fact that the $\Delta$ is not included as an explicit degree of freedom in existing OBE models and is supposed to play only a modest role for NN interactions at low energies, we constructed the NNLO* version of the effective potential [38,39], in which we basically subtracted the $\Delta$ contributions from these LECs and allowed for some fine tuning. This results in numerically reduced values of the $c_{3,4}$:

$$c_3 = -1.15\,\mathrm{GeV}^{-1}, \qquad c_4 = 1.20\,\mathrm{GeV}^{-1}. \tag{3.7}$$

As a consequence, the attraction of the central potential corresponding to chiral TPE is reduced compared to the NNLO calculation of ref. [9]. Differently to the NNLO potential, we also incorporated in the NNLO* version the leading isospin-violating effect due to the pion mass differences in the OPE.

We are now in the position to discuss numerical results of the NNLO* potential. First, we make some general remarks. For NLO (NNLO*), we fit to the Nijmegen $S$- and $P$-wave phases and the $\epsilon_1$ mixing parameter up to $E_{\rm lab} = 50\,(100)$ MeV. These phase shifts at higher energies and for all higher partial waves are therefore predictions. Throughout, we show the phase shifts using the exponential regulator given in eq. (2.9). We are now able to use the same cut-off range as we did at NLO. Varying the cut-off $\Lambda$ between 500 and 600 MeV, we find a weakly changing $\chi^2/$ per degree of freedom. Also, for this range of the cut-off we do not encounter any unphysical bound state in any partial wave, which is in stark contrast to the NNLO results of [9]. We note that one finds an increasing number of such deep bound states with increasing cut-off, eventually leading to a limit cycle behavior (for details, see [3]). The theoretical predictions at NLO and NNLO* for this cut-off range are indicated as bands in the following figures. In most partial waves these bands get thinner when

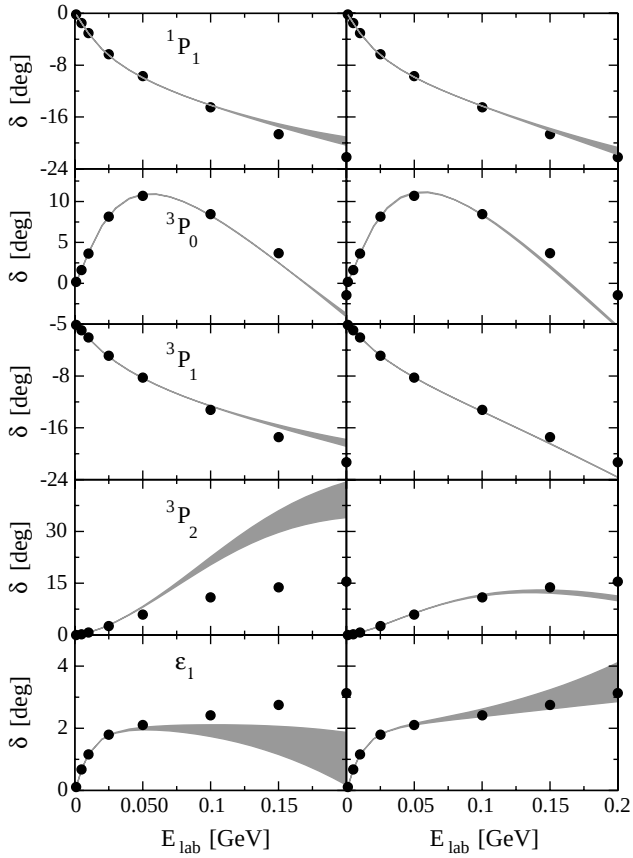


**Fig. 13.** Fits and predictions for the $P$-waves and the mixing parameter $\epsilon_1$ for nucleon laboratory energies $E_{\rm lab}$ below 200 MeV (0.2 GeV). Left/right panels: NLO/NNLO* prediction. The cut-off is chosen between 500 and 600 MeV as shown by the band. The filled circles depict the Nijmegen PSA results.

going from NLO to NNLO* and are also visibly closer to the data (Nijmegen PSA). This is what one expects from a converging EFT.

Let us now regard different partial waves. In fig. 12 we show the two $S$-waves. We find a good description at NNLO* up to 200 MeV, which is comparable with (in case of the $^1S_0$ partial wave slightly worse than) the NNLO results shown in ref. [9].

Consider next the $P$-waves and the mixing angle $\epsilon_1$ shown in fig. 13. The most visible improvement from NLO to NNLO* is observed for $^3P_2$ and $\epsilon_1$. We also note that the description of $^3P_2$ is better than in the NNLO case shown in ref. [9]. While the NNLO corrections to the NLO results for the $^1P_1$, $^3P_1$ and $^3P_2$ partial waves (see fig. 5 in ref. [9]) go in the right directions, the observed effects turn out to be too large and lead to significant deviations from the data. This is cured in the NNLO* version, as can be seen from fig. 13. The NNLO* and NNLO results for the $^3P_0$ partial wave are very similar to each other and to the NLO calculation.

Let us now discuss the $D$-waves and the mixing angle $\epsilon_2$. These are of particular interest since at NNLO* no parameters enter and we already discussed the strong cut-off sensitivity found at NNLO. As shown in fig. 14, this cut-off

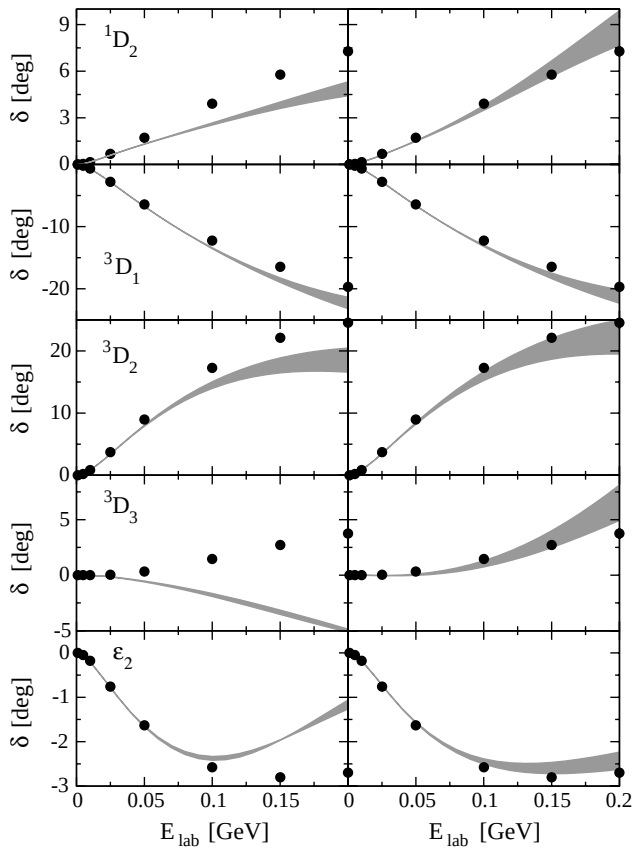


**Fig. 14.** Predictions for the $D$-waves and the mixing parameter $\epsilon_2$ for nucleon laboratory energies $E_{\rm lab}$ below 200 MeV (0.2 GeV). Left/right panels: NLO/NNLO* prediction. The cut-off is chosen between 500 and 600 MeV as shown by the band. The filled circles depict the Nijmegen PSA results.

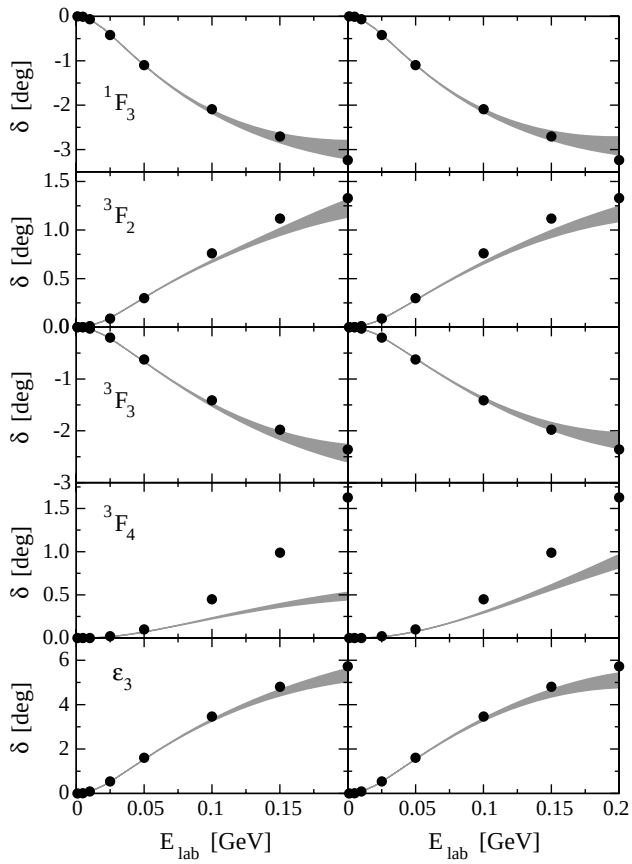


**Fig. 15.** Predictions for the $F$-waves and the mixing parameter $\epsilon_3$ for nucleon laboratory energies $E_{\rm lab}$ below 200 MeV (0.2 GeV). Left/right panels: NLO/NNLO* prediction. The cut-off is chosen between 500 and 600 MeV leading to the band. The filled circles depict the Nijmegen PSA results.

sensitivity is sizeably reduced at NNLO* (in comparison to NNLO) and one obtains an overall good description of all $D$-waves up to laboratory energies of about 200 MeV. We remark that the important $\pi\pi$ correlations which are at the heart of the dramatic improvement in $^3D_3$ from NLO to NNLO* are still present (as in NNLO) since they are driven by the physics behind the LEC $c_1$. Note also the significant improvement for the $\epsilon_2$.

The NNLO* corrections get weaker for $F$- and higher partial waves. In contrast to the strong NNLO effects in the $F$-waves, which cause significant deviations of the phase shifts for the results of the Nijmegen PSA, the NNLO* results can be viewed as small corrections to the NLO calculations, see fig. 15. Indeed, in most cases the difference between the NLO and NNLO* predictions is very small. The only exception is observed for the $^3F_4$ partial wave. Here the NNLO* corrections go in the right direction but are still not sufficient to reproduce the phase shift appropriately at energies larger than 50–100 MeV.

The peripheral partial waves $(G, H, I, \ldots)$ are mostly well described. Most of these are dominated by OPE. However, in very few cases the large values of the $c_i$'s were needed to bring the prediction in agreement with the data, see refs. [27,9]. In the NNLO* potential, the weakened TPE does not provide enough strength as, *e.g.*, seen in $^3G_5$, cf. fig. 16. Similar remarks hold for the $H$ and $I$ phase shifts; we refrain from showing these here.

We now turn to the bound-state (deuteron) properties. We have not fine-tuned the parameters to exactly reproduce the binding energy. It is already described within 2% for the range of cut-offs considered here. In table 1 we collect the deuteron properties at NLO and NNLO* (for $\Lambda =$ 500 and 600 MeV) in comparison to the NNLO results (obtained with an exponential regulator with $\Lambda = 1.05$ GeV) and the CD-Bonn potential (as one generic high-precision potential). Most deuteron properties are well reproduced and improve when going from NLO to NNLO*. We also note that all NNLO* predictions (except the one for the quadrupole moment) are between the NLO and NNLO results[9]. The quadrupole moment is only slightly improved at NNLO*, while the NNLO correction for this quantity goes in the wrong direction. One, however, still observes a discrepancy of about 7% to the experimentally observed

[9] One should keep in mind, that while the NLO and NNLO* results are given within the theoretical uncertainty, which corresponds to a cut-off variation, the results at NNLO are only shown for the optimal choice of the cut-off $\Lambda = 1050$ MeV.

**Table 1.** Deuteron properties derived from our chiral potential at NLO and NNLO* (for the cut-off range considered throughout) compared to the NNLO results of [9], one "realistic" potential and the data. Here, $E_d$ is the binding energy, $Q_d$ the quadrupole moment, $\eta$ the asymptotic $D/S$ ratio, $r_d$ the root-mean-square matter radius, $A_S$ the strength of the asymptotic $S$-wave normalization and $P_D$ the $D$-state probability.

| | NLO | | NNLO* | | NNLO | CD-Bonn | Exp. |
|---|---|---|---|---|---|---|---|
| | 500 MeV | 600 MeV | 500 MeV | 600 MeV | | | |
| $E_d$ (MeV) | −2.152 | −2.165 | −2.182 | −2.189 | −2.224 | −2.225 | −2.225 |
| $Q_d$ (fm$^2$) | 0.265 | 0.266 | 0.265 | 0.268 | 0.262 | 0.270 | 0.286 |
| $\eta$ | 0.0248 | 0.0248 | 0.0247 | 0.0247 | 0.0245 | 0.0255 | 0.0256 |
| $r_d$ (fm) | 1.975 | 1.975 | 1.970 | 1.969 | 1.967 | 1.966 | 1.967 |
| $A_S$ (fm$^{-1/2}$) | 0.862 | 0.866 | 0.871 | 0.874 | 0.884 | 0.885 | 0.885 |
| $P_D$(%) | 3.17 | 3.62 | 3.65 | 4.52 | 6.11 | 4.83 | – |

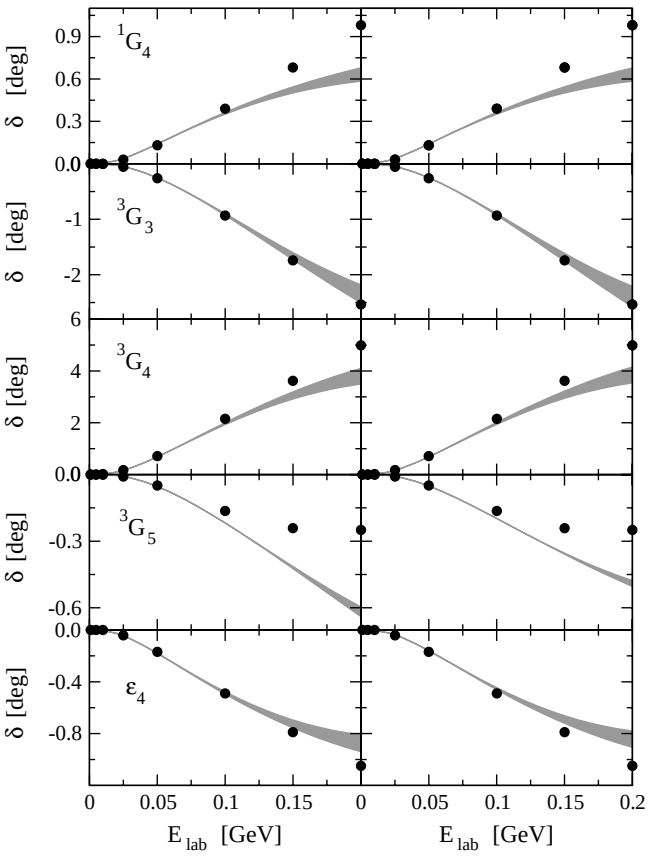


**Fig. 16.** Predictions for the $G$-waves and the mixing parameter $\epsilon_4$ for nucleon laboratory energies $E_{\rm lab}$ below 200 MeV (0.2 GeV). Left/right panels: NLO/NNLO* prediction. The cut-off is chosen between 500 and 600 MeV leading to the band. The filled circles depict the Nijmegen PSA results.

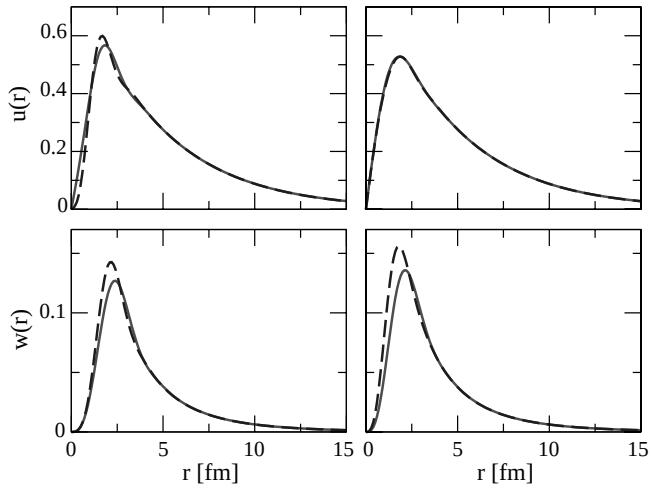


**Fig. 17.** Deuteron wave functions at NLO (left panels) and NNLO* (right panels) in coordinate space. The solid (dashed) lines correspond to the cut-off $\Lambda = 500$ MeV ($\Lambda = 600$ MeV).

value (see, however, the recent discussion by Phillips [40] why this failure is not unexpected). It has also been noted in [41] that fine-tuning the binding energy can slightly improve the prediction for $Q_d$. The NNLO* and NNLO corrections go in the wrong (right) direction for the asymptotic $D/S$ ratio $\eta$ (the asymptotic $S$-wave normalization $A_S$). The improvement for $A_S$ at NNLO* is significant compared to NLO but still leaves space for N$^3$LO corrections. The same holds true for the root-mean-square matter radius $r_d$. We note that the (unobservable) $D$-state probability is reduced as compared to the NNLO result and agrees more with the one found using CD-Bonn potential.

The NNLO* deuteron coordinate space $S$- and $D$-wave functions $u(r)$ and $w(r)$, respectively, are shown in fig. 17. By construction, they have no nodes and agree quite well with, *e.g.*, the CD-Bonn wave functions. This lets one expect that the NNLO* potential when applied to the 3N and 4N systems gives results closer to calculations based on conventional potentials as does NNLO. We will discuss this issue in the following two sections.

Let us now summarize the presented numerical findings for the 2N low-energy observables. Altogether it can be seen that the NNLO* potential leads to results, which are significantly improved compared to the NLO ones and allows for a quantitatively rather good description of the $np$ phase shifts up to $E_{\rm lab} \sim 200$ MeV. While the results for observables at NNLO* and NNLO seem to be of comparable quality and in many cases do not significantly differ from each other, these two versions of the chiral potential suggest quite different scenarios, as discussed above. It is difficult to give preference to the NNLO* or the NNLO

version of the chiral potential. In principle, the LECs $c_i$ should be taken from the analysis of $\pi$N scattering and no readjustment should occur, if sufficiently many terms of the chiral expansion of the $\pi$N scattering amplitude appear in the TPE potential and the $\pi$N parameters are precisely known. However, with the presently available best determinations of these LECs at $Q^2$ and $Q^3$, one gets a very strong attractive central part of the TPE and, as a consequence, encounters unphysical deeply bound virtual states. Further, they lead to an unconventional balance between two- and many-nucleon forces in systems with three (or more) nucleons. On the other hand, boson exchange phenomenology clearly indicates the suppression of contributions with delta intermediate states based on cancellations with, *e.g.*, $\pi\rho$ exchanges. Such a scenario is realized in the NNLO* potential, which does not lead to unphysical bound states in the NN system for reasonable choices of the cut-off. Progress can come from different directions: Further investigations of the $\pi$N system at higher orders in chiral expansion as well as new data (eventually combined in dispersion relations) may allow for more precise determination of the $c_i$'s, so that one would be able to discriminate the physically relevant scenarios of the NN interaction. On the other hand, the final word on the choice of regulator is not yet spoken —one may still contemplate the construction of a coordinate-space regulator that modifies the TPE at short distances such that no unphysical bound states appear. At present, this is only a speculation (we refer to [42] for some related work). Clearly, more work in this direction is mandatory. For the time being we consider it legitimate to use the NNLO* potential in applications to the 3N and 4N systems. For the sake of completeness, we will, however, briefly discuss in the next section NNLO predictions for the 3N system, before we switch to the central issue of this paper and present the NNLO* results for 3N and 4N systems.

## 4 NNLO predictions for the 3N system

As has been shown in [9] the NNLO NN forces describe the Nijmegen NN phase shift values significantly better than the NLO ones. We would like to remind the reader that there occur spurious bound states in $S$-, $P$- and $D$-waves, as already mentioned in the preceeding section. As a consequence of these deeply bound states, the deuteron wave function at NNLO has nodes below about 1 fm, which are not present at NLO (and NNLO*) or using conventional NN forces. In agreement with the correct description of the low-energy $^3S_1$-$^3D_1$ phase shift parameters those nodes also do not influence the low-energy deuteron properties: its binding energy, the asymptotic $D/S$ ratio, the root-mean-square matter radius, the asymptotic $S$-wave normalization constant and the quadrupole moment, which are in good to fair agreement with the experimental values.

In turning to the 3N system one encounters in the Faddeev formulation NN $t$-matrices which are taken off the energy shell. The energy argument is

$$E_2 = E - \frac{3}{4m} q^2, \tag{4.1}$$

where $E$ is the fixed 3N energy and $(3/4m)q^2$ the varying kinetic energy of the third particle in relation to the pair of nucleons interacting via the NN $t$-matrix. Since $q$ varies between 0 and infinity one necessarily hits the spurious bound-state energies, which occur as poles of the NN $t$-operator. Physically spoken this has the consequence that the normal 3N bound state is not stable but decays into two fragments, a deeply bound spurious NN bound state and a nucleon. In practice this decay is rather weak, however, and can be neglected since the physical 3N bound state has little overlap with the short-ranged spurious NN bound state. In addition, one has to expect that there will be spurious 3N bound states at extremely large negative energies in the GeV region. Calculating the 3N observables in the presence of deeply bound spurious states in the NN system requires some precautions. Of course, the ultimate way to calculate 3N observables in the presence of deeply bound NN states would be to treat the poles of the NN $t$-operator explicitly in the corresponding integral equation. The much easier approximate way is to restrict the virtual $q$-values such that $E_2$ does not reach the energies of the spurious bound states, which are in the GeV region. Alternatively, one can transform the two-body Hamiltonian in such a manner that the NN phases do not change but the spurious bound-state energies are moved towards high-positive energies, where they cause no technical obstacles. This can be achieved for instance by the following simple change of the two-nucleon force (starting from the Hamiltonian $H = H_0 + V$):

$$\tilde{V} = V + \sum_i |\Psi_i\rangle \alpha_i \langle \Psi_i| \tag{4.2}$$

leading to the modified Hamiltonian $\tilde{H} = H_0 + \tilde{V}$ with shifted eigenvalues corresponding to spurious eigenstates,

$$\tilde{H}|\Psi_i\rangle = (E_i + \alpha_i)|\Psi_i\rangle, \tag{4.3}$$

where the $\alpha_i$ are sufficiently large-positive energies, $|\Psi\rangle_i$ the spurious bound states and $E_i$ the binding energy of the spurious state $|\Psi_i\rangle$. Note that such a projection does not influence the 2N phase shifts. Also the deuteron wave function remains unchanged.

In this work we do not aim to apply the NNLO potential to the 3N and 4N systems and only want to demonstrate that one needs strong 3NFs to describe the data. The approximate methods described above are therefore sufficient for our present purpose. We solved the 3N Faddeev equation for the triton using $\tilde{V}$ instead of $V$ and this for NNLO. With the cut-off $\Lambda = 1000\,\mathrm{MeV}$ in the NN system we found for triton binding energy $E = -3.8\,\mathrm{MeV}$. This number turned out to be nearly independent of the actual values of $\alpha_i$ (which are of the order of a few GeV). A very close value arises if on sticks to the original NN force $V$ at NNLO and restricts the range of $q$-values as mentioned above. One has to conclude that this form of

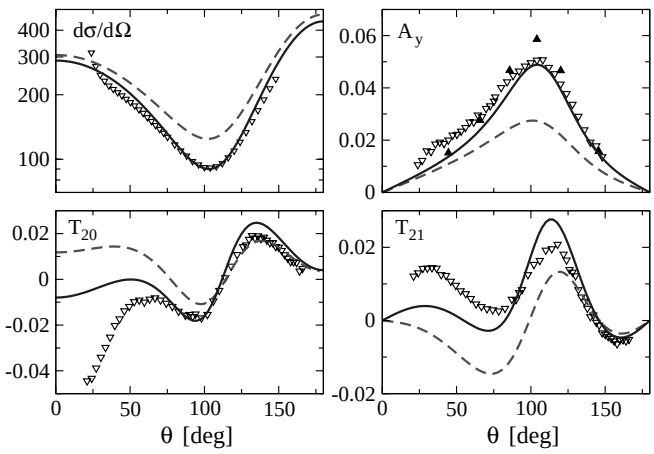


**Fig. 18.** Differential cross-section (in (mb/sr)) and analyzing powers $A_y$, $T_{20}$ and $T_{21}$ for elastic *nd* scattering at $E_{\rm lab} = 3\,$MeV. The solid and dashed lines correspond to predictions based on the CD-Bonn and NNLO potentials. The open (filled) triangles are *pd* [43,44] (*nd* [45]) data.

the NN force requires strong 3N forces to account for the missing binding energy. Notice, however, that these required 3N forces may still be much weaker than the corresponding 2N ones. Indeed, we found an expectation value for the potential energy in the triton at NNLO of about $-172\,$MeV, which is much larger than the one observed for various high-precision potentials of the order $-40$ to $-50\,$MeV[10]. The corresponding large value for the kinetic energy has, in principle, to be expected due to the additional nodes in the deuteron and triton wave functions in the short-distance range, which are caused by the deeply bound states.

In view of the results for the triton binding energy one also has to expect that theoretical 3N scattering observables based only on the NNLO NN force (*i.e.* neglecting the 3NFs) will be in conflict with the data. This is indeed the case as shown in fig. 18 for a few examples.

Thus, we conclude that taking into account only the 2N interaction at NNLO and neglecting the corresponding 3NFs does not allow for a correct description of the 3N observables. This presumably will be corrected by the inclusion of the 3N forces, which because of consistency in the power counting has to be taken into account at NNLO. It will be interesting in the future to check this statement explicitely.

## 5 3N and 4N predictions with the NNLO* NN potential

We use the Faddeev-Yakubovsky scheme to solve for the 3N and 4N bound states and the 3N scattering observables as described in [8,46]. The calculations are fully converged with respect to the number of partial-wave states and standard numerical discretizations. Table 2 shows the results for the 3N and 4N binding energies using the NLO and the NNLO* NN potentials. Note that for the NLO version the numbers slightly different from the ones published in [7] appear since we have now taken into account the leading isospin-violating effect due to the charged-to-neutral pion mass difference in the OPE.

**Table 2.** Theoretical $^3$H and $^4$He binding energies for different cut-offs $\Lambda$ at NLO and NNLO* compared to the AV-18 and CD-Bonn predictions (point Coulomb interaction perturbatively removed), the experimental $^3$H binding energy and the Coulomb corrected $^4$He binding energy in MeV. The kinetic energies $T$ (in MeV) and $S$-, $P$- and $D$-state probabilities for $^4$He are also shown.

| Potential | $E(^3\mathrm{H})$ | $E(^4\mathrm{He})$ | $T$ | $S$ (%) | $P$ (%) | $D$ (%) |
|---|---|---|---|---|---|---|
| NLO, 500 | −8.544 | −29.57 | 61.4 | 94.71 | 0.07 | 5.22 |
| NLO, 600 | −7.530 | −23.87 | 77.6 | 92.60 | 0.11 | 7.29 |
| NNLO*, 500 | −8.590 | −29.96 | 62.2 | 93.65 | 0.10 | 6.25 |
| NNLO*, 600 | −8.245 | −27.87 | 64.9 | 90.61 | 0.17 | 9.22 |
| AV-18 | −7.628 | −24.99 | 97.8 | 85.89 | 0.35 | 13.76 |
| CD-Bonn | −8.013 | −27.05 | 77.2 | 89.06 | 0.22 | 10.72 |
| Exp. | −8.48 | −29.00 | – | – | – | – |

We see a clear reduction of the cut-off dependence in going from NLO to NNLO*, as it is expected from a converging EFT. For reasons of comparison, we also display the kinetic energy and the probabilities of the various ground-state components $(S, P, D)$ in $^4$He. The resulting binding energies for NNLO* are near the experimental data and larger than the values typically achieved with conventional potentials. The results for two representatives, AV-18 and CD-Bonn, are also displayed in table 2. Note that the NNLO* results encompass the experimental values, quite in contrast to the realistic potentials. We remark, however, that the chiral NN forces employed up to now are for the *np* system and therefore do not yet take all relevant isospin-violating effects into account[11]. Experience tells us that this leads to an unphysical increase in the binding energy of about 200 keV (1 MeV) in $^3$H ($^4$He). Nevertheless, in relation to conventional forces one ends up close to the experimental data for $^3$H and $^4$He using the NNLO* NN potential and consequently will need smaller contributions of 3N forces than using conventional NN forces.

For 3N scattering we show in figs. 19–24 elastic *nd* scattering observables for laboratory energies of 3, 10 and 65 MeV, in order, and in fig. 25 *nd* break-up cross-sections for two arbitrarily selected kinematical configurations at $E_{\rm lab} = 13\,$MeV. In each case the NLO are compared to the NNLO* predictions and the ones based on the modern high-precision potentials. Like for the bound-state energies we find in all cases a much reduced cut-off dependence for NNLO* in comparison to NLO. Also, at the highest energy we considered, 65 MeV, one observes now a strong improvement compared to the NLO results, which in some cases deviate significantly from the data. We also

[10] Thus, the missing binding energy of about 4 MeV for the triton to be provided by 3N forces is still much smaller compared to the strength of the 2N interaction.

[11] Such effects can be dealt with in nuclear EFT as discussed, *e.g.*, in [11].

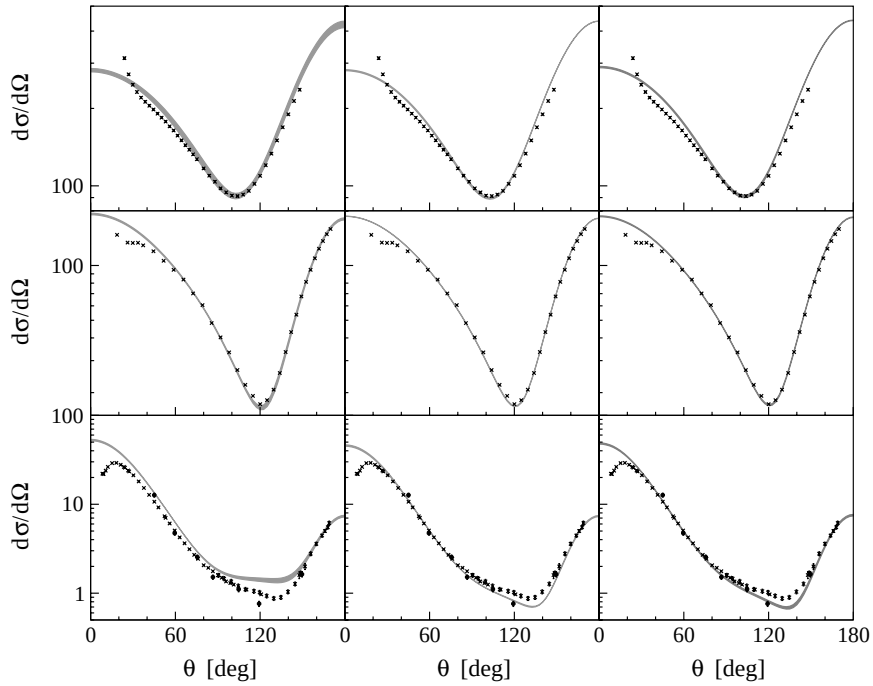


**Fig. 19.** Differential cross-section for elastic *nd* scattering in (mb/sr) for $E_{\rm lab} = 3, 10, 65$ MeV (top to bottom). Results at NLO (left panel) and NNLO* (middle panel). The bands correspond to the range $\Lambda = 500$ to 600 MeV. Results based on the high-precision potentials (CD-Bonn, AV-18, Nijm-93, Nijm-I,II) are shown in the right panel. Here the bands refer to the spread in predictions using the various potentials. The crosses are *pd* data: at 3 MeV from [43], at 10 MeV from [47], and at 65 MeV from [48]. The circles at 65 MeV are *nd* data from [49].

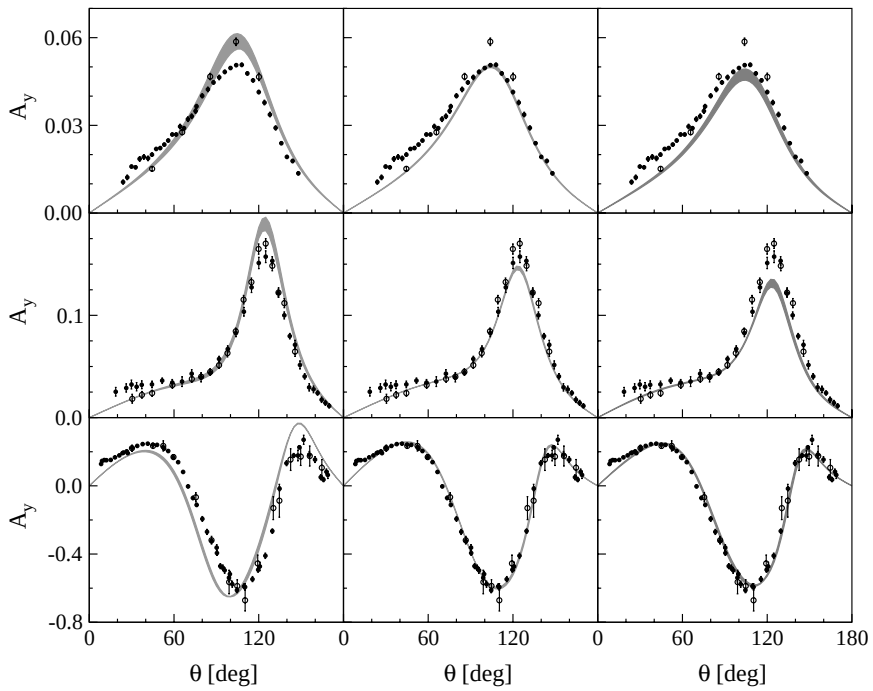


**Fig. 20.** Analyzing power $A_y$ for elastic *nd* scattering, for $E_{\rm lab} = 3, 10, 65$ MeV (top to bottom). Data at 3 MeV are from [45] (*nd*, open circles) and [44] (*pd*, filled circles), at 10 MeV from [50] (*nd*, open circles) and [47] (*pd*, filled circles), and at 65 MeV from [49] (*nd*, open circles) and [48] (*pd*, filled circles). For further notations, see fig. 19.

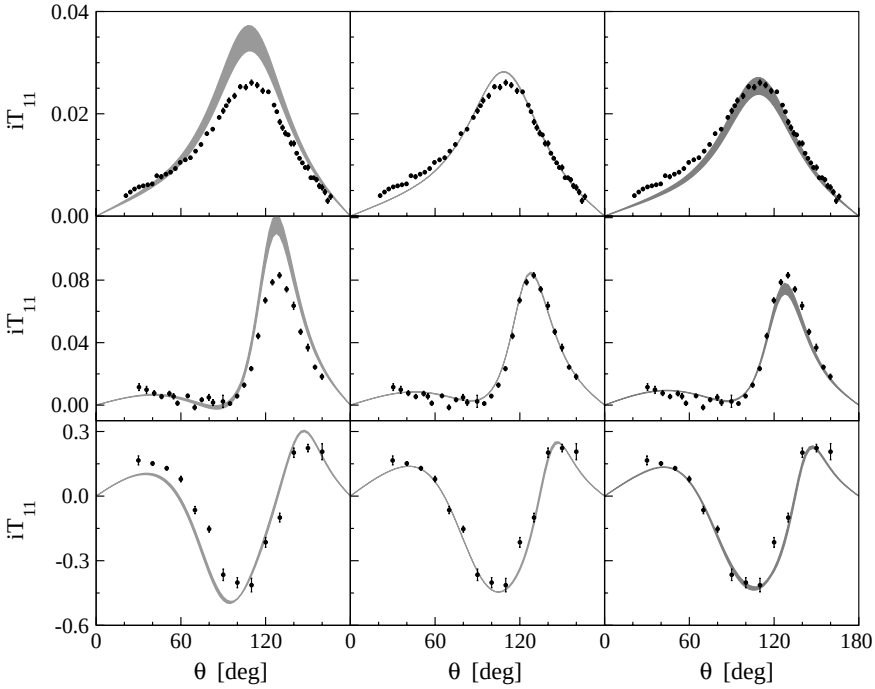


**Fig. 21.** Tensor-analyzing power $iT_{11}$ for elastic *nd* scattering, for $E_{\rm lab} = 3, 10, 65$ MeV (top to bottom). The circles are *pd* data: at 3 MeV from [44], at 10 MeV from [47], and at 65 MeV from [51]. For further notations, see fig. 19.

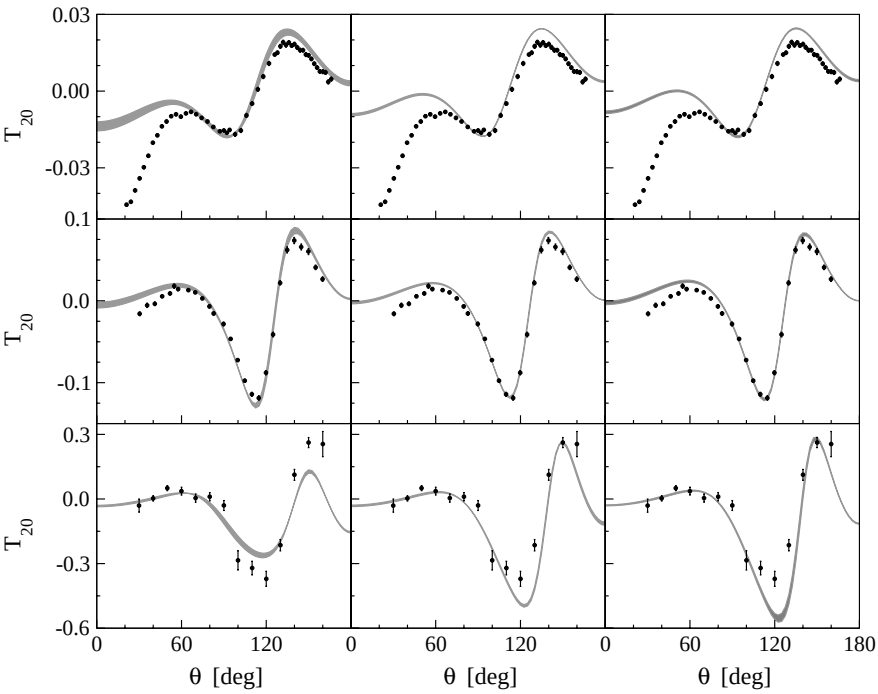


**Fig. 22.** Tensor-analyzing power $T_{20}$ for elastic *nd* scattering, for $E_{\rm lab} = 3, 10, 65$ MeV (top to bottom). The circles are *pd* data: at 3 MeV from [44], at 10 MeV from [47], and at 65 MeV from [51]. For further notations, see fig. 19.

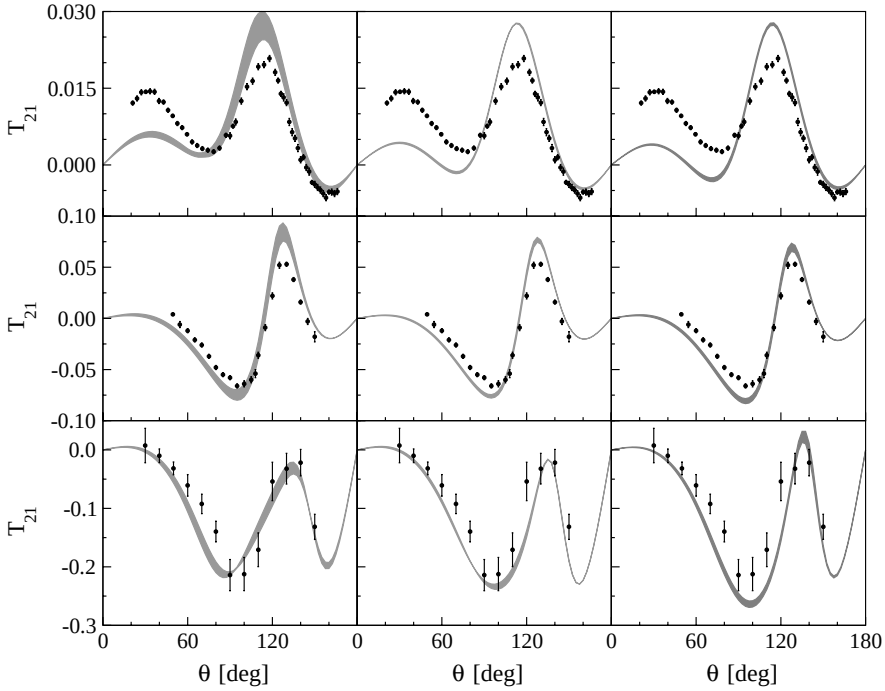


**Fig. 23.** Tensor-analyzing power $T_{21}$ for elastic *nd* scattering, for $E_{\rm lab} = 3, 10, 65\,$MeV (top to bottom). The circles are *pd* data: at 3 MeV from [44], at 10 MeV from [47], and at 65 MeV from [51]. For further notations, see fig. 19.

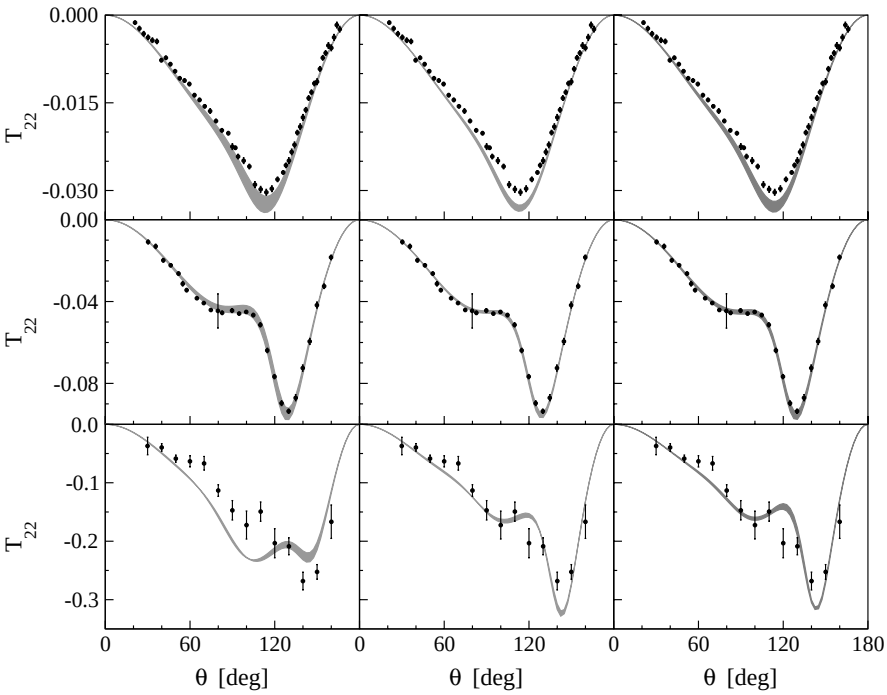


**Fig. 24.** Tensor-analyzing power $T_{22}$ for elastic *nd* scattering, for $E_{\rm lab} = 3, 10, 65\,$MeV (top to bottom). The circles are *pd* data: at 3 MeV from [44], at 10 MeV from [47], and at 65 MeV from [51]. For further notations, see fig. 19.

**Table 3.** $^3P_j$ $np$ phase shifts at NLO and NNLO* for the smallest and largest values of the cut-off compared to the phases based on the CD-Bonn potential [52] and to the Nijmegen PSA [26].

| $T_{\rm lab}$ (MeV) | NLO | | NNLO* | | CD-Bonn | NPSA |
|---|---|---|---|---|---|---|
| | 500 MeV | 600 MeV | 500 MeV | 600 MeV | | |
| $^3P_0$ | | | | | | |
| 1 | 0.19 | 0.19 | 0.17 | 0.17 | 0.18 | 0.18 |
| 5 | 1.68 | 1.67 | 1.59 | 1.58 | 1.61 | 1.63(1) |
| 10 | 3.74 | 3.72 | 3.62 | 3.58 | 3.62 | 3.65(2) |
| 25 | 8.28 | 8.22 | 8.26 | 8.16 | 8.10 | 8.13(5) |
| 50 | 10.90 | 10.84 | 11.12 | 11.01 | 10.74 | 10.70(9) |
| 100 | 8.27 | 8.31 | 8.34 | 8.43 | 8.57 | 8.46(11) |
| 150 | 2.52 | 2.52 | 1.88 | 2.15 | 3.72 | 3.69(14) |
| 200 | −3.70 | −4.11 | −5.43 | −5.23 | −1.55 | −1.44(17) |
| $^3P_1$ | | | | | | |
| 1 | −0.12 | −0.12 | −0.11 | −0.11 | −0.11 | −0.11 |
| 5 | −0.99 | −0.99 | −0.91 | −0.92 | −0.93 | −0.94 |
| 10 | −2.17 | −2.16 | −2.02 | −2.02 | −2.04 | −2.06 |
| 25 | −5.05 | −5.03 | −4.82 | −4.83 | −4.81 | −4.88(1) |
| 50 | −8.35 | −8.32 | −8.22 | −8.23 | −8.18 | −8.25(2) |
| 100 | −12.61 | −12.66 | −13.49 | −13.47 | −13.23 | −13.24(3) |
| 150 | −15.56 | −15.94 | −18.48 | −18.43 | −17.51 | −17.46(5) |
| 200 | −17.80 | −18.86 | −23.64 | −23.65 | −21.38 | −21.30(7) |
| $^3P_2$ | | | | | | |
| 1 | 0.02 | 0.02 | 0.02 | 0.02 | 0.02 | 0.02 |
| 5 | 0.24 | 0.24 | 0.25 | 0.25 | 0.26 | 0.25 |
| 10 | 0.70 | 0.70 | 0.71 | 0.71 | 0.72 | 0.71 |
| 25 | 2.87 | 2.89 | 2.64 | 2.65 | 2.60 | 2.56(1) |
| 50 | 8.05 | 8.29 | 6.29 | 6.34 | 5.93 | 5.89(2) |
| 100 | 20.32 | 22.60 | 11.31 | 11.70 | 11.01 | 10.94(3) |
| 150 | 29.73 | 35.97 | 12.11 | 13.04 | 13.98 | 13.84(4) |
| 200 | 34.02 | 44.30 | 9.92 | 11.31 | 15.66 | 15.46(5) |

observe that the theoretical uncertainty due to the cut-off variation is sometimes smaller than the spread using the various phase equivalent conventional potentials. Note that most of the deviations of the theoretical predictions from the $pd$ data in case of the tensor-analyzing powers and the differential cross-section at low energies and at forward angles are due to the Coulomb $pp$ force [53].

Let us now take a closer look at the calculated elastic observables. The differential cross-section at NNLO* agrees well with the data and with the predictions based upon various high-precision potentials, cf. fig. 19, and is strongly improved at 65 MeV compared to the NLO results. The vector-analyzing power of elastic $nd$ scattering at low energies is well known to be underpredicted by the standard NN potential models, see fig. 20, right panel, and this remains true even after inclusion of the existing 3N forces based on boson exchanges. As reported in ref. [7] and shown in the left panel of fig. 20, the NLO predictions at 3 MeV are essentially in agreement with the data, while at 10 MeV one even observes a slight overestimation in maximum. The NLO results for $A_y$ at 65 MeV show significant deviations from the data. Our predictions at NNLO* are much closer to the results based upon the high-precision potentials, *i.e.* the data are underpredicted at low energies (3 and 10 MeV) and reproduced accurately at higher ones (65 MeV), cf. fig. 20. Although some improvement with respect to the predictions based upon the high-precision potentials can be seen at 3 and especially at 10 MeV, the pending puzzle is now back at NNLO*. As pointed out in ref. [54], one possible reason for the significant change of about 20% in the $A_y$ predictions when going from NLO to NNLO* may be the deviations of the $np$ $^3P_j$ phase shifts from the data at NLO. These channels are well known to be very important for the $nd$ $A_y$, see, *e.g.*, [8]. In table 3 we demonstrate that these partial waves are now much better described at NNLO*. We also remind the reader that in contrast to high-precision potential models, which are constructed to perfectly reproduce the NN data below the pion production threshold, in EFT one does not aim at a perfect description of the data by increasing the phenomenological content of the NN interaction but rather at performing systematic order-by-order calculations. At each specific order in the low-energy expansion (in our case chiral expansion) one has some theo-

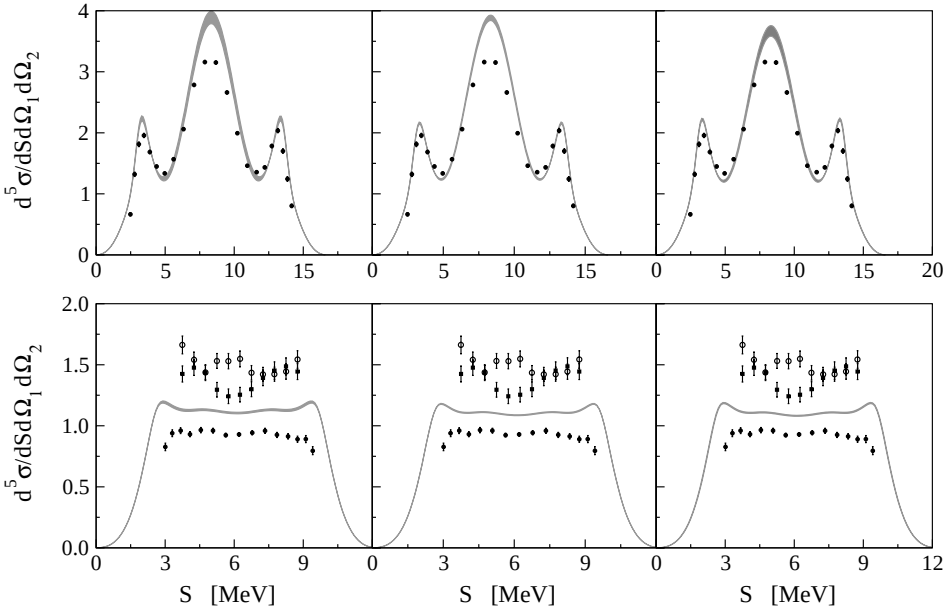


**Fig. 25.** 3N break-up cross-sections in (mb/MeV/sr$^2$) against the arc length $S$ of the kinematically allowed locus. The *pd* data (filled circles) [55] show in the upper row a peak (in the middle) related to a quasi-free scattering picture. The two sets of *nd* data from [56] (open circles) and [57] (filled squares), upper group, and the *pd* data, lower ones, are at and in the neighborhood of "space-star" configuration.

retical error due to missing higher-order terms, which can be estimated. Considering our results for $A_y$ at NLO one should therefore keep in mind the level of precision of the NLO approximation. Further, since the *nd* $A_y$ is a very sensitive observable and is strongly affected by changing the *np* $^3P_j$ phase shifts by only few percent, the large uncertainty for this specific observable has to be expected in the EFT approach.

The situation with the deuteron vector-analyzing power $iT_{11}$ is very similar to the one with $A_y$. This is shown in fig. 21[12]. The NNLO* predictions for the tensor-analyzing powers $T_{20}$ and $T_{21}$ at 3 and 10 MeV as well as for $T_{22}$ at all three energies follow the band made up from the variations among the high-precision potentials. Remarkably, our results for $T_{20}$ and $T_{21}$ are even significantly closer to the data at 65 MeV.

In case of the specific 3N break-up results shown in fig. 25 the chiral force predictions are equally off the data as the predictions of the conventional forces. In case of the upper row the deviations in the quasi-free peak to the *pd* data might be due to Coulomb force effects, whose precise size is still unknown. The lower row addresses the space-star anomaly. We underestimate significantly the two sets of *nd* data, which are also far off the *pd* data. As in the case of elastic-scattering observables the NNLO* predictions follow the band made up from the various high-precision potentials. Again the size of Coulomb force effects is unknown. For more information on these break-up configurations see refs. [8,56].

[12] Notice that only *pd* data exist for this observable. Inclusion of the Coulomb interaction will lead to significant underestimation of the $iT_{11}$ [53].

It is also interesting to compare our results to the ones shown in ref. [54], in which the same *nd* scattering observables have been calculated using the phenomenological high-precision extension of the chiral potential by Entem and Machleidt [30]. In fact, our results for these observables show a remarkable similarity to the ones presented in this reference, *i.e.* both predictions agree with the calculations based upon the conventional high-precision potential models and with the data in most cases and are slightly closer to the data for $T_{20}$ and $T_{21}$ at 65 MeV. The only significant differences between our results and the ones of ref. [54] are observed for $A_y$ (and $iT_{11}$) at low energies (3 and 10 MeV), which are slightly improved in case of the NNLO* version. It is very gratifying to see that at least up to $E_{\rm lab} = 65$ MeV our NNLO* potential with 11 adjustable parameters works for *nd* scattering equally well as the one of ref. [30] with 46 adjustable parameters. This remarkable agreement may serve as a nice demonstration of the power and the advantage of an EFT with consistent power counting compared to more phenomenological approaches: performing chiral expansion of the nuclear force up to some definite order by inclusion of *all* relevant diagrams and counter terms allows to describe low-energy observables with the same precision regardless of the kind of system the theory is applied to (2N, 3N,...). From the point of view of EFT, it makes not much sense to improve the description of the 2N observables alone by a phenomenological extension of the short-range part of the NN force. As one can see comparing figs. 19–24 with the corresponding ones of ref. [54], this does not lead to an improvement in describing other systems at low energy (*i.e.* the 3N system). In order to reduce the theoretical uncertainty, one should instead go to higher orders,

which requires the inclusion of 3N, 4N, ..., interactions as well as more pion exchanges in the 2N force. Furthermore, the whole concept of developing phenomenological NN potentials, which reproduce the NN data perfectly with $\chi^2$/datum = 1 is in conflict with the general EFT philosophy: at each fixed finite order of the low-energy expansion one necessarily has some definite uncertainty in description of observables. Adjusting the cut-off parameters in various partial waves to improve the fit to data, as has been done in ref. [30], is not acceptable from the point of view of pure EFT, where the cut-off dependence of observables may serve as an estimation of the theoretical error.

It is now an urgent task to encode the three topologically different 3N forces, which have to be taken into account at NNLO (NNLO*) and to determine the corresponding parameters in the 3N system. Pioneering studies in [58] indicate that specifically the diagram in fig. 5 of this reference might have a chance to solve the $A_y$ puzzle. This extensive work will be dealt with in a forthcoming paper.

## 6 Summary

The concept and the resulting NN forces at LO, NLO and NNLO of $\chi$PT have been reviewed. Our approach is based on the method of unitary transformation applied to the most general chirally invariant Hamiltonian expressed in terms of pion and nucleon fields. This method leads to energy-independent nuclear forces, a property which is important for the application to more than two nucleon systems. The NNLO NN forces driven by the low-energy constants $c_{1,3,4}$ lead to deeply bound unphysical NN states in low partial waves if the values $c_{1,3,4}$ are taken from typical $\pi$N data analysis[13]. While this has no negative observable consequences in the NN system, since the spurious NN bound-state energies are outside the realm of validity of $\chi$PT, they lead to a scenario for nuclear physics which is quite different from the one driven by conventional nuclear forces. First, the central part of the NN potential turns out to be much more attractive as is expected from conventional approaches. Further, the predictions for 3N, 4N, ..., binding energies based upon the purely NN forces are much lower, far below the experimental values, and 3N scattering observables deviate dramatically from the data. Therefore, unlike for conventional NN forces, which to a very large extent describe the data, and 3N forces are only needed as a relatively small additional contribution, the 3N force contributions here will be very essential. We provided arguments based upon experiences with meson theoretical potentials supporting the choice of $c_{3,4}$ constants, which are numerically smaller and where intermediate $\Delta$ contributions are subtracted out. Based on those values we introduced a novel NNLO* NN force which describes NN phase shifts with comparable quality as the NNLO one up to about $E_{\rm lab} = 200\,$MeV. These NNLO* potential is free of spurious bound states and leads to predictions in the 3N and 4N systems which are rather close to the ones familiar from conventional high-precision NN forces. It is now of highest interest to include the 3N forces which should be taken into account at that order in $\chi$PT. This work is in preparation.

In contrast to conventional nuclear forces this chiral approach is systematic in the sense of power counting and nuclear forces are expected to be constructed in a convergent scheme. Therefore the step to NNNLO should be performed in order to see whether convergence can be reached and long pending problems with conventional forces like the low-energy analyzing power $A_y$ can be solved without *ad hoc* assumptions.

[13] Note that this statement might not hold true for different regularization schemes.

We would like to thank Joanna Kurós-Żołnierczuk for helping us in creating various figures. This work was supported by the Deutsche Forschungsgemeinschaft (E.E.), the U.S. National Science Foundation under Grant No. PHY-0070858 (A.N.) and the Polish Committee for Scientific Research under Grant No. 2P03B02818 (H.W.). The calculations have been performed on the T90 and the T3E of the NIC Jülich, Germany.

## References

1. P.G. Lepage, in *Particles and Fields*, edited by J.C.A. Barata *et al.* (World Scientific, Singapore, 1998) (arXiv:hep-ph/9706029).
2. S.R. Beane *et al.*, Phys. Rev. A **64**, 042103 (2001).
3. E. Epelbaum, U.-G. Meißner, in preparation.
4. S. Weinberg, Phys. Lett. B **251**, 288 (1990); Nucl. Phys. B **363**, 3 (1991).
5. C. Ordóñez, L. Ray, U. van Kolck, Phys. Rev. C **53**, 2086 (1996).
6. E. Epelbaoum, W. Glöckle, U.-G. Meißner, Nucl. Phys. A **637**, 107 (1998).
7. E. Epelbaum *et al.*, Phys. Rev. Lett. **86**, 4787 (2001).
8. W. Glöckle *et al.*, Phys. Rep. **274**, 109 (1996).
9. E. Epelbaum, W. Glöckle, U.-G. Meißner, Nucl. Phys. A **671**, 295 (2000).
10. U. van Kolck, Thesis, University of Texas at Austin, 1993, unpublished.
11. M. Walzl, U.-G. Meißner, E. Epelbaum, Nucl. Phys. A **693**, 663 (2001).
12. S.N. Yang, W. Glöckle, Phys. Rev. C **33**, 1774 (1986).
13. U. van Kolck, Phys. Rev. C **49**, 2932 (1994).
14. V. Bernard, N. Kaiser, U.-G. Meißner, Int. J. Mod. Phys. E **4**, 193 (1995).
15. V. Bernard, N. Kaiser, U.-G. Meißner, Nucl. Phys. B **457**, 147 (1995).
16. V. Bernard, N. Kaiser, U.-G. Meißner, Nucl. Phys. A **615**, 483 (1997).
17. M. Mojžiš, Eur. Phys. J. C **2**, 181 (1998).
18. N. Fettes, U.-G. Meißner, S. Steininger, Nucl. Phys. B **640**, 199 (1998).
19. P. Büttiker, U.-G. Meißner, Nucl. Phys. A **668**, 97 (2000).
20. N. Fettes, U.-G. Meißner, Nucl. Phys. A **676**, 311 (2000).
21. R. Koch, Nucl. Phys. **448**, 707 (1986).
22. E. Matsinos, Phys. Rev. C **56**, 3014 (1997).
23. SAID on-line program, R.A. Arndt *et al.*, see website `http://gwdac.phys.gwu.edu/`.

24. T. Becher, H. Leutwyler, JHEP **0106**, 017 (2001).
25. M.C.M. Rentmeester, R.G.E. Timmermans, J.L. Friar, J.J. de Swart, Phys. Rev. Lett. **82**, 4992 (1999).
26. V.G.J. Stoks, R.A.M. Klomp, M.C.M. Rentmeester, J.J. de Swart, Phys. Rev. C **48**, 792 (1993).
27. N. Kaiser, R. Brockmann, W. Weise, Nucl. Phys. A **625**, 758 (1997).
28. N. Kaiser, S. Gerstendörfer, W. Weise, Nucl. Phys. A **637**, 395 (1998).
29. E. Epelbaum, Doctoral Thesis, published in *Berichte des Forschungszentrum Jülich*, No. 3803 (2000).
30. D.R. Entem, R. Machleidt, Phys. Lett. B **524**, 93 (2002).
31. R. Machleidt, K. Holinde, Ch. Elster, Phys. Rep. **149**, 1 (1987).
32. E.E. van Faassen, J.A. Tjon, Phys. Rev. C **28**, 2354 (1983).
33. G. Janssen, K. Holinde, J. Speth, Phys. Rev. C **54**, 2218 (1996).
34. T.R. Hemmert, B.R. Holstein, J. Kambor, J. Phys. G **24**, 1831 (1998).
35. K. Holinde *et al.*, Phys. Rev. C **18**, 870 (1978).
36. T. Becher, H. Leutwyler, Eur. Phys. J. C **9**, 643 (1999).
37. M.R. Robilotta, Phys. Rev. C **63**, 044004 (2001).
38. E. Epelbaum *et al.*, in AIP Conf. Proc., Vol. **603**, Issue 1 (AIP, 2001) p. 17.
39. E. Epelbaum, U.-G. Meißner, W. Glöckle, Ch. Elster, Phys. Rev. C **65**, 044001 (2002).
40. D.R. Phillips, in AIP Conf. Proc., Vol. **603**, Issue 1 (AIP, 2001) p. 149.
41. M. Walzl, U.-G. Meißner, Phys. Lett. B **513**, 37 (2001).
42. S.R. Beane, P.F. Bedaque, M.J. Savage, U. van Kolck, Nucl. Phys. A **700**, 377 (2002).
43. K. Sagara *et al.*, Phys. Rev. C **50**, 576 (1994).
44. S. Shimizu *et al.*, Phys. Rev. C **52**, 1193 (1995).
45. J.E. McAninch *et al.*, Phys. Lett. B **153**, 29 (1985).
46. H. Kamada, W. Glöckle, Nucl. Phys. A **548**, 2005 (1992).
47. F. Sperisen *et al.*, Nucl. Phys. A **422**, 81 (1984).
48. H. Shimizu *et al.*, Nucl. Phys. A **382**, 242 (1982).
49. H. Rühl *et al.*, Nucl. Phys. A **524**, 337 (1991).
50. W. Tornow *et al.*, Phys. Rev. Lett. **49**, 312 (1982).
51. H. Witała *et al.*, Few-Body Systems **15**, 67 (1993).
52. R. Machleidt, Phys. Rev. C **63**, 024001 (2001).
53. A. Kievsky, S. Rosati, M. Viviani, Phys. Rev. C **64**, 041001 (2001).
54. D.R. Entem, R. Machleidt, H. Witała, Phys. Rev. C **65**, 064005 (2002).
55. G. Rauprich *et al.*, Nucl. Phys. A **535**, 313 (1991).
56. H.R. Setze *et al.*, Phys. Lett. B **388**, 229 (1996).
57. J. Strate *et al.*, J. Phys. G: Nucl. Phys. **14**, L229 (1988).
58. D. Hüber, J.L. Friar, A. Nogga, H. Witała, U. van Kolck, Few-Body Systems **30**, 95 (2001).